Biogeosciences Discuss., doi:10.5194/bg-2015-661, 2016
Manuscript under review for journal Biogeosciences
Published: 7 March 2016

Predicting carbon dioxide and energy fluxes across global FLUXNET sites with regression algorithms

Gianluca Tramontana[1], Martin Jung[2], Gustau Camps-Valls[3], Kazuhito Ichii[4,5], Botond Raduly[1,6], Markus Reichstein[2], Christopher R. Schwalm[7], M. Altaf Arain[8], Alessandro Cescatti[9], Gerard Kiely[10], Lutz Merbold[11], Penelope Serrano-Ortiz[12], Sven Sickert[13], Sebastian Wolf[14] and Dario Papale[1].

[1]Department for Innovation in Biological, Agro-food and Forest systems (DIBAF), Univeristy of Tuscia, Viterbo, 01100, Italy,

[2]Max Planck Institute for Biogeochemistry, Jena, 07745, Germany;

[3]Image Processing Laboratory (IPL), Paterna (València), 46980, Spain.

[4]Department of Environmental Geochemical Cycle Research, Japan Agency for Marine-Earth Science and Technology, Yokohama, 236-0001, Japan.

[5]Center for Global Environmental Research, National Institute for Environmental Studies, Tsukuba, 305-8506, Japan.

[6]Department of Bioengineering Sapientia Hungarian University of Transylvania, Miercurea Ciuc, 530104, Romania.

[7]Woods Hole Research Center, Falmouth MA, 02540, USA.

[8]School of Geography and Earth Sciences, McMaster University, Hamilton (Ontario), L8S4L8, Canada

[9]Institute European Commission, Joint Research Centre, Institute for Environment and Sustainability, Ispra, Ispra, 21027, Italy

[10]Civil & Environmental Engineering and Environmental Research Institute, University College, Cork, T12 YN60, Ireland.

[11]Department of Environmental Systems Science, Institute of Agricultural Sciences, ETH Zurich, Zurich, 8092, Switzerland.

[12]Department of Ecology, University of Granada, Granada, 18071, Spain.

[13]Computer Vision Group, Friedrich Schiller University Jena, 07743 Jena, Germany

[14]Department of Environmental Systems Science, ETH Zurich, Zurich, 8092, Switzerland.

Correspondence to: G. Tramontana (g.tramontana@unitus.it)

Abstract. Spatial-temporal fields of land-atmosphere fluxes derived from data-driven models can complement simulations by process-based Land Surface Models. While a number of strategies for empirical models with eddy covariance flux data have been applied, a systematic intercomparison of these methods has been missing so far. In this study, we perform a cross-validation experiment for predicting carbon dioxide (CO_2), latent heat, sensible heat and net radiation fluxes, in different ecosystem types with eleven machine learning (ML) methods from four different classes (kernel methods, neural network, tree methods, and regression splines). We employ two complementary setups: (1) eight days average fluxes based on remotely sensed data, and (2) daily mean fluxes based on meteorological data and mean seasonal cycle of remotely sensed variables. The pattern of predictions from different ML and setups were very consistent. There were systematic differences in performance among the fluxes, with the following ascending order: net ecosystem exchange (R^2<0.5), ecosystem respiration (R^2>0.6), gross primary production (R^2>0.7), latent heat (R^2>0.7), sensible heat (R^2>0.7), net radiation (R^2>0.8). ML methods predicted very well the across sites variability and the seasonal cycle (R^2> 0.7) of the observed fluxes, while the eight days deviations from the mean seasonal cycle were not well predicted (R^2< 0.5). Fluxes were better predicted at forested and temperate climate sites than at ones growing in extreme climates or less representated in training data (e.g. the tropics). The large ensemble of ML based models evaluated will be the basis of new global flux products.

Keywords: Machine learning, carbon fluxes, energy fluxes, FLUXNET, remote sensing, FLUXCOM

1. Introduction

Improving our knowledge of the carbon, water, and energy exchanges between terrestrial ecosystems and the atmosphere is essential to better understand and model Earth's climate system (IPCC, 2007; Reich, 2010). In situ continuous observations

can be obtained by the eddy covariance technique, which estimates the net exchanges of carbon dioxide (CO_2), water vapour and energy between land ecosystems and the atmosphere (Aubinet at al., 2012; Baldocchi et al., 2014). Under ideal conditions eddy covariance estimations are equals to the vertical turbulent fluxes plus the changes in the scalar storage under the measurement height, while under the non-ideal conditions advection needs to be accounted (Aubinet et al., 2005, Hammerle et al., 2007).

The large-scale measurement network, FLUXNET integrates site observations of these fluxes globally and provides detailed time series of carbon and energy fluxes across biomes and climates (Baldocchi et al., 2008). However, eddy-covariance measurements are site-level observations, and spatial upscaling is required to estimate these fluxes at regional to global scales.

The increasing number of eddy covariance sites across the globe has encouraged the application of data-driven models by machine learning (ML) methods such as Artificial Neural Networks (ANNs, Papale et al., 2003), Random Forest (RF, Tramontana et al., 2015), Model Trees (MTE, Jung et al., 2009; Xiao et al., 2008, 2010) or Support Vector Regression (SVR, Yang et al., 2006, 2007) to estimate surface-atmosphere fluxes from site level to regional or global scales (e.g. Beer et al., 2010, Jung et al., 2010, 2011; Kondo et al., 2015; Schwalm et al., 2010; Yang et al., 2007; Xiao et al., 2008, 2010). The ML upscaled outputs are also increasingly used to evaluate land surface models (e.g., Anav et al., 2013; Bonan et al., 2011; Ichii et al., 2009; Piao et al., 2013).

The key characteristic of data-driven models compared the process-based ones are the former's intrinsic observational nature, and that functional relationships are not prescribed but rather emerge from the patterns found in the measurements. In this context, data-driven models extract multivariate functional relationships between the in situ measured fluxes of the network and explanatory variables in an empirical way. The explanatory variables are generally coming from satellite remote sensing, providing information on vegetation state (e.g., vegetation indices) and other land surface properties (e.g., surface temperature), along with continuous measurements of meteorological variables at flux towers.

While ML-based upscaling provides a systematic approach to move from point-based flux estimates to spatially explicit gridded fields, various sources of uncertainty exist. For example, individual ML methods might have different responses especially when these models are applied beyond the conditions sampled by the training dataset (Jung et al., 2009; Papale et al., 2015). The information content of the driving input variables may not be sufficient to capture the variability of the fluxes in all conditions (Tramontana et al., 2015). Moreover, remotely sensed and meteorological gridded datasets are affected by uncertainties themselves. Remote sensing data contain noise, biases and gaps, and can be perturbed by atmospheric effects or by the presence of snow. Meteorological gridded datasets are known to contain product specific biases (Garnaud et al., 2014; Tramontana et al., 2015; Zhao et al., 2012).

Thorough experiments using multiple data-driven models and explanatory variables are an essential step to identify and assess limitations and sources of uncertainty in the empirical upscaling approach. In this study, we present and evaluate an ensemble of ML based empirical models to predict CO_2 and energy fluxes across FLUXNET sites. The participating models were selected in the context of the FLUXCOM initiative, forming the basis of subsequent global flux products. We performed a consistent cross-validation for two complementary experimental setups using: (1) eight days average fluxes based on remotely sensed data, and (2) daily mean fluxes based on remotely sensed and meteorological data. The ML tools have spanned the full range of commonly applied algorithms: from model tree ensembles, multiple adaptive regression splines, artificial neural networks, to kernel methods, with several representatives of each family. The different ML algorithms were trained with consistent sets of predictor variables. Our overarching aim was to understand how well fluxes of CO_2 (gross primary production (GPP), terrestrial ecosystem respiration (TER) and net ecosystem exchange (NEE)), and energy (latent heat (LH), sensible heat (H) and net radiation (Rn)) could be predicted by an ensemble of ML methods. More specifically, we addressed the following questions:

1. Were the patterns of predicted fluxes consistent between the two experimental setups?

Biogeosciences Discuss., doi:10.5194/bg-2015-661, 2016
Manuscript under review for journal Biogeosciences
Published: 7 March 2016

2. How different were the predictions of the various ML algorithms?
3. How did the performance differ among capturing the across-sites, seasonal and the deviations from the mean seasonal cycle variability?
4. How did the performance differ among climate zones or ecosystem types?

2. Material and methods

2.1 Data

2.1.1 Eddy covariance study sites

We used eddy covariance data from 224 flux-tower sites (supplementary material, Sect. S1), which originate from the FLUXNET La Thuile synthesis dataset and CarboAfrica network (Valentini et al., 2014). The study sites were distributed globally and cover most plant functional types (PFT) and biomes over the globe (Table 1, Giri et al., 2005).

2.1.2 Observation-based CO_2 and energy fluxes

All flux measurements were post-processed using standardized procedures of quality control and gap-filled following Reichstein et al. (2005) and Papale et al. (2006). Estimates of GPP and TER were derived from half-hourly NEE measurements using two independent flux partitioning methods: (1) following Reichstein et al. (2005), where the temperature sensitivity of ecosystem respiration was initially estimated from night-time NEE data and then extrapolated to daytime to estimate TER and GPP, by subtracting NEE (negatively signed for the CO_2 uptake) from TER; (2) following Lasslop et al. (2010), where daytime NEE data were used to constrain an hyperbolic light response curve to directly estimate GPP and TER. In the following we reference GPP and TER derived by Reichstein et al. (2005) as GPP_R and TER_R; whereas estimates based on the Lasslop et al. (2010) method are referred to as GPP_L and TER_L.

The half-hourly data were aggregated to daily values and screened according to multiple quality criteria, as follow:

1) we excluded data when more than 20% of the data were based on gap-filling with low confidence (Reichstein et al., 2005);

2) we identified and removed obviously erroneous periods due to non-flagged instrument or flux partitioning failures based on visual interpretation;

3) we excluded data-points where the two flux-partitioning methods provided extremely different patterns. Specifically, we computed for each site a robust linear regression between (a) $TER_R - GPP_L$ and NEE, and (b) GPP_R and GPP_L. Data points with a residual outside the range of ± 3 times of the inter-quartile range were removed. This criterion removed only the extreme residuals, systematic differences between methods were not removed;

4) we removed the 5% of data-points with the largest friction velocity (u*) uncertainty, defined as data points above the 95th percentile of daily u* uncertainty (measured as the inter-quartile range of 100 bootstrap samples).

Similarly to the CO_2 fluxes, we applied the same criteria 1) and 2) for the energy fluxes. Additionally, we removed data with inconsistent energy fluxes, i.e. when the residual of a robust linear regression between LE + H and Rn for each site was outside three-times the inter-quartile range of the residuals.

2.1.2 Remote sensing data

We collected data coming from Moderate Resolution Imaging Spectroradiometer (MODIS) which provided data at a spatial resolution of 1km or better (Justice et al., 2002). We used the cutout surroundings of 3×3 km pixels centered on the towers. We collected and processed the following MODIS products: MOD11A2 Land Surface Temperature (LST; Wan et al., 2002),

Biogeosciences Discuss., doi:10.5194/bg-2015-661, 2016
Manuscript under review for journal Biogeosciences
Published: 7 March 2016

MOD13A2 Vegetation Index (Normalized Difference Vegetation Index (NDVI) and Enhanced Vegetation Index (EVI); Huete et al., 2002), MOD15A2 Leaf Area Index (LAI) and Fraction of Absorbed Photosynthetic Active Radiation (FPAR; Myneni et al., 2002), and MCD43A2 and MCD43A4 Bidirectional Reflectance Distribution Function (BRDF) corrected surface reflectances (Schaaf et al., 2002). The BRDF-corrected surface reflectance data were further processed to calculate the Normalized Difference Water Index (NDWI) (Gao, 1996) and the Land Surface Water Index (LSWI) (Xiao et al., 2002). These data were obtained from http://daac.ornl.gov/MODIS/.

The remote sensing data were further processed to improve data quality and data gaps were filled to create continuous time-series data, and to minimize non-land surface signals. We adopted the following processing scheme: we identified good quality pixels by the using the quality assurance/quality criteria (QA/QC) included in the MODIS product. If more than 25% of the pixels had good quality at the time of snapshot, the average of good quality pixels were assigned as the actual value. Otherwise, the data at the time snapshot were marked as blank (no data). Then, we created the mean seasonal variations from 2000-2012 using only good pixels data and the data gaps in the processed data were filled using the mean seasonal variation. Only MOD13 was provided with 16 days composite, and eight days data were created by assigning the 16 days composite value to the corresponding two eight days periods.

2.1.3 Meteorological data

The in situ measured air temperature (Tair), global radiation (Rg), VPD, and precipitation were used after data screening according to the criteria 1) and 2) as for the measured fluxes (see Sect. 2.1.2). We also used long-term time series of these variables from ERA-Interim for the period 1989-2010 (Dee et al., 2011), which were bias-corrected for each site on the basis of the overlapping period of in situ measurements (see http://www.bgc-jena.mpg.de/~MDIwork/meteo/). These long-term meteorological data were primarily used to calculate consistent metrics of climatological variables (e.g. mean annual temperature) across all sites given the temporal coverage of data of the different sites. In addition, we used a composite of these ERA-Interim data based and in situ measured data to obtain a gap-free time series for calculating a simple soil Water Availability Index (WAI, see Sect. 2.3.2 and supplementary material, Sect. S3).

2.2 Participating ML methods

For our purpose, 11 ML algorithms for regression from four broad families were chosen: tree-based methods, regression splines, neural networks, kernel methods. Moreover a comprehensive review of ML algorithms in biophysical parameter estimation can be found in Verrelst et al. (2015). At follow a brief description of the characteristics of each family.

Tree based methods

These methods construct hierarchical binary decision trees. The inner nodes of the tree hold decision rules according to explanatory variables (e.g. less/greater than X1), recursively splitting the data into subspaces. The leaf nodes at the end of the decision tree contain models for the response variable. Because a single tree is generally not effective enough to cope with strong non-linear multivariate relationships, ensembles of trees are often used. We applied two different tree ensemble methods: (1) Random Forests (RF) which combines regression trees grown from different bootstrap samples and randomly selected features at each split node (Breiman, 2001; Ho, 1998); and (2) Model Tree Ensembles (MTE) which combine model trees (Jung et al., 2009). The main difference between regression and model trees is the prediction model in the leaf node: a simple mean of the target values from the training in regression trees and a parametric function (here a multiple linear regression) in model trees. In this study, we used three different variants of MTE, which differ mainly with respect to different cost functions for determining the splits, and the technique to create the ensemble of model trees. Further details are described in the supplementary material (Sect. S2).

Regression splines

Multivariate regression splines (MARS) are an extension of simple linear regression adapted to non-linear response surfaces using piecewise (local) functions. The target variable is predicted as the sum of regression splines and a constant value (Alonso Fernández, 2013; Friedman et al., 1991).

Neural networks

Neural networks are based on nonlinear and nonparametric regressions. Their base unit is the neuron, where nonlinear regression functions are applied. The neurons are interconnected and organized in layers. The output of *m* neurons in the current layer are the inputs for *n* neurons of the next layer. We used two types of neural networks: the artificial neural network (ANN) and the group of method for data handle (GMDH). In an ANN, each neuron performs a linear regression followed by a non-linear function. Neurons of different layers are interconnected by weights that are adjusted during the training (Haykin et al., 1999; Papale et al., 2003). The GMDH is a self-organizing inductive method (Ungaro et al., 2005) building polynomials of polynomials; the neurons are pairwise connected through a quadratic polynomial to produce new neurons in the next layer (Shirmohammadi et al., 2015).

Kernel methods

Kernel methods (Shawe-Taylor and Cristianini, 2004) owe their name to the use of kernel functions, which measures similarities between input data examples. Among the available kernel methods we used: (1) support vector regression (SVR) (Vapnik et al., 1997), (2) kernel ridge regression (KRR) (Shawe-Taylor and Cristianini, 2004), and (3) Gaussian process regression (GPR) (Rasmussen, 2006; Verrelst et al., 2012). The SVR defines a linear prediction model over mapped samples to a much higher dimensional space, which is non-linearly related to the original input (Verrelst et al., 2012, Yang et al., 2007). The KRR is considered as the kernel version of the regularized least squares linear regression (Shawe-Taylor and Cristianini, 2004, Verrelst et al., 2012). The GPR is a probabilistic approximation to nonparametric kernel-based regression, and both a predictive mean (point-wise estimates) and predictive variance (error bars for the predictions) can be derived. We also used a hybrid approach combining RF with simple decision stumps in the inner nodes and GPR for prediction in the leaf nodes (Fröhlich et al., 2012).

2.3 Experimental design

2.3.1. Experiment setups

We defined two complementary experimental setups, which differ in the choice of explanatory variables, and the temporal resolution of the target fluxes: 1) at eight days temporal resolution using exclusively remote sensing data (hereafter RS); and 2) at daily temporal resolution using meteorological data together with the mean seasonal cycle (MSC) of remote sensing data (hereafter RS+METEO). In the latter case, the MSC of remote sensing data were smoothed and interpolated to daily time step. Each setup was characterized by advantages and disadvantages. While RS could provide products with high spatial resolution (up to 1km), data were limited to the MODIS era (2000-present) and had a coarse temporal resolution. The uncertainties of remote sensing data at tower locations, due to finer scale spatial heterogeneity, also degraded the performance of the ML methods. RS+METEO could take advantage of information from meteorological variables, and was resistant to the noise of remote sensing time series because only mean seasonal cycle of data from satellite were used. RS+METEO allowed for upscaled products over a longer time period (because not constrained by the availability of MODIS data) and finer time scale (daily). However the predictive skill of this setting was conditioned by the missing of information regarding the interannual variability of vegetation greenness. In addition the use of meteorological gridded datasets introduced another source of uncertainty coming from potential dataset specific biases and by their typically coarse spatial resolution (0.5 degrees or larger).

2.3.2. Variable selection

Biogeosciences Discuss., doi:10.5194/bg-2015-661, 2016
Manuscript under review for journal Biogeosciences
Published: 7 March 2016

Combining remote sensing and meteorological data (see Sect. 2.1.2 and 2.1.3) we created additional variables for model inputs. In the case of RS+METEO setup we derived the Water Availability Index (WAI) that it was based on a simple soil water balance model (for more details see supplementary material, Sect. S3) as an attempt to better represent water stressed conditions. For both setups we derived proxies for absorbed radiation as the product between vegetation greenness (e.g. EVI, NDVI, FPAR) and drivers related to the absorbable energy for photosynthesis (e.g. daytime LST, Rg, and potential radiation). Other derived variables included the mean seasonal cycle (MSC) of dynamic variables and associated metrics (minimum, maximum, amplitude, and mean). For remote sensing predictors, the MSC and associated metrics were based on the period 2001-2012 while for climate variables were based on the bias corrected daily long-term ERA-Interim data reference period (1989-2010). In total, 216 potential explanatory variables were created for RS and 231 for RS+METEO (see supplementary material S4 for details).

For each setup we selected a small subset of variables best suited to predict the target fluxes using a variable selection search algorithm. Variable selection was an important component in the spatial upscaling because the accuracy of predictions improves and the computational costs of the global predictions were minimized. We used the Guided Hybrid Genetic Algorithm (GHGA) published by Jung and Zscheischler (2013), which was designed for variable selection problems with many candidate predictor variables and computationally expensive cost functions. The GHGA required the training of a regression algorithm (here RF) to estimate the cost associated with selected variable subsets (see S5 for details).

Instead of doing a computationally demanding variable selection for each individual flux, variable selection runs were performed for the RS and RS+METEO setups and separately for CO_2 and energy fluxes. This procedure had the advantage that the resulting global products originated from a consistent set of predictor variables. All trained machine learning used the same drivers for predictions and they were listed in Table 2.

2.3.3. Model training

The capability of ML methods to spatially extrapolate CO_2 and energy fluxes was evaluated by a 10-fold cross-validation strategy. The training datasets were stratified into 10-folds, each one roughly containing 10% of the data. Entire sites were assigned to each fold (Jung et al., 2011). The training of machine learning was done using data of nine folds while the prediction was done for the remaining one. This operation was repeated 10 times and each one of the 10 fold was used exactly once as validation set. In this way: a) the validation sets were completely independent from the training sets, b) the validation of the models was done to the entire dataset. Due to computational expense of the RS+METEO setup, only one method representing each "family" – multiple regressions, RF, MARS, ANN and KRR – was trained.

ML methods base settings were tuned before the training (for further details, see supplementary material S6). These hyper-parameters accounted for regularization in order to avoid overfitting, as well as for the shape and smoothness constraints. Instead, the model parameters were estimated for each ML every time in each fold

2.3.4. Model evaluation

In order to highlight the differences between the RS and RS+METEO setups, the daily output from RS+METEO were aggregated to eight days time steps; the same periods and sites were used for the comparison. Besides the statistical analysis of the individual ML cross-validation results, we focused on the ensemble median estimate, here defined as the median predicted value across all ML for a given setup and time step. The advantages of the median ensemble estimate was the robustness of the predictions for the contribution of many ML that reduced the risk of outlier in the extrapolation exercise.

We used different metrics to evaluate the ML performance such as the Nash and Sutcliffe model efficiency (MEF), the root mean square error (MSE), the empirical BIAS, the Pearson's linear correlation coefficient (ρ), the coefficient of determination (R^2) and the ratio of variance (ROV).

Biogeosciences Discuss., doi:10.5194/bg-2015-661, 2016
Manuscript under review for journal Biogeosciences
Published: 7 March 2016

MEF (Nash and Sutcliffe, 1970) was the capability of a model to estimate a target variables better than a reference model. If the reference model was the mean value of the observation, MEF was calculated as:

$$MEF = 1 - \frac{\sum_{i=1}^{n}(x_i - y_i)^2}{\sum_{i=1}^{n}(y_i - \bar{y})^2} \quad (1)$$

where X_i and Y_i were the predicted and the observed values respectively and $\bar{y}$ is the mean value of the observations. MEF varied between -inf to 1; in the case of MEF > 0 the predictive skill of the model was better than the mean (MEF = 1 for the ideal model), instead if MEF=0 the predictive skill of the model was equivalent to the mean, finally if MEF < 0, the predictive skill of the mean value of the target was better than the model.

The RMSE was estimates as the root square of the mean value of the squared residuals:

$$RMSE = \sqrt{\frac{\sum_{i=1}^{n}(x_i - y_i)^2}{n}} \quad (2)$$

The BIAS was evaluated as the mean value of model's residuals

$$BIAS = \frac{\sum_{i=1}^{n}(x_i - y_{i)}}{n} \quad (3)$$

Following Gupta et al. (2009) the importance of bias on the overall uncertainty was evaluated as the ratio between the square of BIAS and the Mean Square Error, the latter estimated as the square value of RMSE.

The Pearson's linear correlation coefficient (ρ) was the ratio between the covariance between the modeled and observed values (σ_{xy}) and the product of the standard deviation of modeled (σ_x) and observed (σ_y) values:

$$\rho = \frac{\sigma_{xy}}{\sigma_x \sigma_y} \quad (4)$$

R^2 was estimated as the squared value of ρ; finally ROV was evaluated as the ratio between predicted and observed standard deviation.

We evaluated the overall predictive skill of the models, evaluating the consistency among trained ML approaches and across the experimental setup. Then we evaluated the capability of the regression models to predict site-specific mean fluxes, mean seasonal cycle (MSC), and anomalies (Jung et al., 2011). The MSC per site was calculated using the averaged values for each eight days period across all available years, but only when at least two values (i.e., years) for each eight days period were available. To assess the mean values of the study sites, we calculated the mean of the MSC if at least 50% of the 46 eight days values were present, whereas the eight days anomalies were calculated as the deviation of a flux value from the MSC. Finally, the mean site value was removed from the MSC to disentangle the seasonal variation from the mean site values, making them as complementary.

We also analyzed the performance for the different Köppen climate zone and IGBP plant functional types. In particular. we computed for each flux, setup and tower site the performances of ML median estimate. Then, for each setup, we estimated the median value of the site-by-site statistics per PFT and climate zone.

3. Results and Discussions

Biogeosciences Discuss., doi:10.5194/bg-2015-661, 2016
Manuscript under review for journal Biogeosciences
Published: 7 March 2016

3.1 Overview

The ensemble median estimate always outperformed the median performance of ML-specific methods (the median value of metrics calculated for individual ML) (Table 3; Appendix A). Individual ML methods also exhibited higher skill than multiple linear regressions (higher MEF and lower RMSE; Fig. 1). This highlighted the added value of ML methods as these were able to account for nonlinearities in either explanatory variables or fluxes. Overall, using the ensemble median estimate gave a representative overview of ML-based flux predictions.

3.2 Predictive skill of CO_2 and energy fluxes

Predictive skill of the ensemble median estimate clustered into tiers whereby energy fluxes were uniformly better predicted than CO_2 fluxes: Rn > H/LE/GPP > TER > NEE (Table 3). The highest skill levels as exhibited by net radiation showed near perfect agreement; Rn displayed a model efficiency (MEF) of 0.91-0.92 and a correlation of 0.96. The decline in skill for the second tier fluxes was ca. 15% to 20%; MEF for H, LE, and GPP is 0.79, 0.75-0.76, and 0.71 respectively. The lowest two tiers exhibited 20% and 40% declines in MEF (0.57-0.64 and 0.43-0.46 for TER and NEE respectively). These relative rankings were unchanged regardless of skill metric used—apart from RMSE where the difference in fluxes units and magnitude, confounded a direct comparison (Table 3)—suggesting that accuracy and precision scale linearly.

There were only minor performance differences between the two CO_2 fluxes partitioning methods (Table 3), although for the RS setup, the performance of TER_L were comparatively lower than TER_R (lower MEF, ρ and ROV). A similar trend was not found in the case of RS+METEO setup.

The overall skill profile in this study confirmed previous upscaling efforts (Jung et al., 2011; Yuan et al., 2010). This relatively stable cross-study skill gradient reflected the information content of the available predictor variables. The spatiotemporal variability of remotely sensed land surface properties was well-suited to predict the top tier fluxes (Rn, H, LE, and GPP) (Jung et al., 2008; Tramontana et al., 2015; Xiao et al., 2010;.Yang et al., 2007)

The higher skill associated with energy fluxes suggested that these fluxes were more easily predictable using the drivers selected in particular respect to NEE. In fact NEE was strongly controlled by external factors such management and disturbances (Amiro et al., 2010; Thornton et al., 2002) and by lag and memory effects (Bell et al., 2012; Frank et al., 2015, Papale et al., 2015; Paruelo et al., 2005), which were both poorly captured by predictor variables typically used in upscaling and poorly constrained in general, i.e., data limited. Another reason for the low performances in NEE simulation was in the random uncertainties of the measurements that were larger compared to H and LE and had an important effect being NEE the difference between two large components (GPP and TER).

Among the CO_2 fluxes, GPP was the best predicted probably because the seasonal cycle and canopy properties, which were strongly related to GPP, were well represented by the ML drivers. The intermediate skill of TER, relative to CO_2 fluxes only, was supported by its tight coupling to the well-predicted GPP and the availability of predictor variables that captured the temperature dependency of respiration. However specific drivers for TER could be still missing. In fact in contrast to GPP, the canopy properties were less important drivers of TER, while the soil properties, carbon pools and their turnover rates were key for respiratory processes (Amiro et al., 2010) but not available to be used as drivers. This likely explains the poor performance for TER in comparison with GPP.

3.3 Were the flux predictions consistent between RS and RS+METEO?

Skills, in terms of both performance tiers and absolute value of skill metrics, were similar for both RS and RS+METEO approaches with some differences, in particular: (1) RS and RS+METEO diverged more for those fluxes where they showed lower overall skill levels, in particular the NEE (Fig. 1, Table 3); (2) MEF and correlation values were slightly larger for RS than RS+METEO, excluding TER_L where the opposite was found, indicating an important role of the meteorological data for

Biogeosciences Discuss., doi:10.5194/bg-2015-661, 2016
Manuscript under review for journal Biogeosciences
Published: 7 March 2016

this version of the ecosystem respiration. It should be considered that the differences in performances could be also due to a different ensemble size, with the RS composed of 11 individual ML-based ensemble members, whereas RS+METEO was based on only four. The overall good performance of the RS setup implied that CO_2 and energy fluxes can be mapped exclusively based on remotely sensed inputs allowing high-spatial resolution products and reduction of uncertainty due to the meteorological drivers spatialization (Tramontana et al., 2015).
Nonetheless, the differences between the experimental setups were less appreciable.

3.4 How different were the predictions of the various ML algorithms?

Pair-wise R^2 values for model outputs (Table 4) were close to unity ($R^2 \geq 0.90$), regardless of experimental setup, with NEE showing a slightly lower value ($R^2 = 0.84$). Among corresponding model residuals (Table 4), R^2 values ranged from 0.79 (Rn) to 0.89 (TER_L). Comparing the same ML technique but using different experimental setups (Table 4, RS vs. RS+METEO) showed similarly high, albeit somewhat diminished level of consistency (R^2 range ranged from 0.71 to 0.80 for model residuals). These finding highlighted that the ML methods were mapping between explanatory variables and target fluxes both reliably and robustly. Across the all three consistency checks there was also a tendency for better predicted fluxes (e.g., H) to exhibit higher pair-wise R^2 values than poorly predicted fluxes (e.g., NEE). This was expected as more robust patterns—and therefore those that lead to greater predictive skill—were easier to extract regardless of ML algorithm and experimental setup in this study; thus increasing consistency. While this broad consistency confirmed that the extracted patterns were robust, the decline in R^2 when comparing the same ML trained with different drivers (RS vs RS+METEO) respect to the correlation among ML methods with the same drivers, suggested that the choice of the explanatory variable had higher impact than the choice of the ML technique for the pattern of predictions.

3.5 How did the performance differ among capturing the across-sites, seasonal and the deviations from the mean seasonal cycle variability?

Decomposing FLUXNET data into across-sites variability, mean seasonal cycle, and interannual variability components (Sect. 2.3.4) revealed clear gradients in predictive skill (Table 5 and Fig. 2). Across-sites variability was in general well-captured by the ML (R^2 range: 0.61 to 0.81 except for NEE) and the best predicted pattern were found for GPP and TER. This suggests that ML were suitable to reproduce the spatial pattern of mean annual fluxes.
The variability in the mean seasonal cycle (at eight days time scale) was also uniformly well predicted (R^2 between 0.67-0.77 for GPP and TER, and between 0.86-0.98 for the energy fluxes) and the best predicted pattern for energy fluxes in particular for LE and Rn.
The importance of seasonality in CO_2 and energy annual fluxes was known (Joiner et al., 2014; Jung et al., 2011; Merbold et al., 2009; Wolf et al., 2011) and biases in its dynamic (e.g. in the growing season length) could lead to biases into the predicted fluxes (Ichii et al., 2010). A clear benefit of the ML upscaling approach used here was that none of the parameters controlling seasonality were prescribed, reducing the possibility of biases.
In contrast, the eight days anomalies variability were generally poorly captured by all the ML approaches used with only H and Rn showing an R^2 greater than 0.4. This low predictive skill held regardless of whether eight days, monthly (Jung et al., 2011), or annual time steps were used (data not shown). This was likely due to a combination of missing predictor variables (e.g. disturbances, management, legacy effects) and the noise/uncertainty in both predictor and target variables that played a major role when small differences (like in the interannual variability) were predicted. The slightly better performances when sensible heat flux was estimated could be due to the lower uncertainty in this flux respect to the others (only one sensor used, the sonic anemometer, in contract with the other fluxes where also the gas analyzer was used) but also to the fact that it was

Biogeosciences Discuss., doi:10.5194/bg-2015-661, 2016
Manuscript under review for journal Biogeosciences
Published: 7 March 2016

strongly and directly related to the LST used as driver. In any case, predicting interannual variability remained one of the largest challenges in the context of empirical upscaling.

NEE was confirmed to be the most difficult and consequently poorest predicted flux (Table 3). NEE showed considerably lower skill relative to the other fluxes for across-sites variability (R^2 = 0.46), the mean seasonal cycle (R^2 = 0.59), and interannual variability (R^2 = 0.13, TER_L was the lowest at 0.10).

3.6 How did the performance differ among climate zones or ecosystem types?

Using climate zone and plant functional type (PFT) to disaggregate ML methods performances we found that in general energy fluxes were better predicted than CO_2 fluxes among the different climate zone and PFTs (Fig. 3 and Appendix C). The median R^2 between simulation and observation for CO_2 fluxes (excluding NEE) was greater than 0.6 for more than 75% of the PFT and climate zone, while in the energy fluxes the R^2 greater was higher than 0.7 for more than the 85% of the PFT and climate zone (in all sites for Rn).

NEE was again consistently poorly predicted (low R^2 and high relative RMSE; Fig. 3), apart from deciduous broadleaf forests (DBF) and MF where a marginal improvement was evident. The better performance in these two vegetation types could be related to the higher seasonal variance of NEE in comparison with the other PFTs that was a pattern more consistent with the seasonal variance of the used drivers.

Overall the ML methods showed poor prediction capability in the tropics and in the evergreen broadleaf forests (EBF). Possible explanations were the absence of a clear seasonal cycle traceable by the remote sensing signal (evergreen vegetation) and a low variance in their seasonal cycle that was challenging to explain mathematically and capture with a model. (Sims et al., 2008; Yebra et al., 2015; Yuan et al., 2010). In addition, the difficulty in acquiring cloud-free remotely sensed data, from one introduced additional uncertainty in the drivers.

Reason for low performances could be also the lack of important driving variables, that were probably the main explanation for cropland, where management information were missing (e.g. irrigation, fertilization, tillage) and also for cold and dry environments where the extreme nature of the environments characterized by water limitation (for dry sites) and the extreme low temperature (for cold sites) required more targeted drivers such direct estimations of soil water content. In addition, cold and dry sites were characterized by both low magnitude and low variance of fluxes, making difficult to explain the fluxes variability in these ecosystems types by empirical models.

4. Conclusions

The ML methods presented and evaluated in this study have shown high capability to predict CO_2 and energy fluxes, in particular the between-site variability and the seasonal variations, with a general tendency of increasing performance in the following order: NEE, TER, GPP, LE, H, and Rn. The relatively poor performance for NEE likely resulted from factors that cannot be easily accounted for in ML based modelling approaches, such as legacies of site history (e.g. disturbances, management, age and stocks). Future progress in this direction requires the reconstruction of the relevant management and disturbance history, trying to integrate information from forest inventories, high resolution satellites such LANDSAT and high resolution biomass data from radar and LIDAR with the aim to improve model performance. The better results obtained for the energy fluxes (LE and H) in comparison to the CO_2 fluxes (GPP and TER) could be related to more complex mechanisms driving the carbon cycle that were also not represented in the drivers used, in addition to a relatively higher uncertainties in the GPP and TER due to the use of flux partitioning methods based on NEE measurements.

We found no substantial bias in the predictions of the ML models for most vegetation types or biomes. However, the predictions have deviated more from the observations for evergreen broadleaf forests, croplands, the tropics and extreme climates. The growing number of eddy-covariance sites, in particular new sites in poorly represented regions will likely

improves the predictive skill in the future. This is particularly relevant since tropical areas account for a disproportionate share of the global water and carbon cycle (Beer et al., 2010).

The deviations from the mean seasonal cycle (eight days anomalies) are still poorly captured by the ML methods. We expected the RS+METEO approach to perform better regarding the prediction of anomalies as meteorological drivers were included and the noise in remote sensing time series was greatly reduced by using smoothed seasonal cycle. However, this was not the case, which indicates that either, the eight days anomalies of both, the flux data, and the drivers, were strongly affected by the uncertainties, or that the anomalies were dominated by management and disturbance (or other factors) not accounted for in the predictors. Hence, the prediction of interannual anomalies remains a major unresolved research topic.

The predictions for ecosystem fluxes across FLUXNET by different ML techniques and by different explanatory variable sets (RS vs RS+METEO) were highly consistent, indicating that the extracted patterns by the trained models were robust, realistic and not subject to severe overfitting. The differences in predictions among the RS and RS+METEO setups were slightly larger than among different ML methods, suggesting that future activities should concentrate on identifying new driver variables to further improve the performance of fluxes predictions. Nevertheless, we recommend using the ensemble median estimate of multiple ML techniques for analyzing global flux products because extrapolation beyond the FLUXNET-sampled conditions may generate larger differences among methods than discernible from our cross-validation comparison.

The ML based models presented and extensively evaluated here form the basis of an extensive archive of global gridded flux products, which is currently under development. The thorough cross-validation experiment presented in this paper helps users understanding the products' strengths and weaknesses. The good performance of the ML methods, the availability of an ensemble of them, and the detailed analysis of their uncertainties will make this archive an unprecedented data stream to study the global land-atmosphere exchange of CO_2, water and energy.

Appendix A: Median performance of the methods.

In table A1 we reported, for both setups, the median value of skill metrics (MEF, RMSE, and absolute value of BIAS) realized by singular ML and their related variability such estimated as the median absolute deviation (MAD) from the median multiplied per 1.4826 (see Jung et al., 2009 for details)

Appendix B: scatterplot between the observations and the predictions by the median ensemble of ML.

In Fig. B1 and B2 we reported the scatterplots between eddy covariance observations and the modeled median ensemble estimates respectively for RS and RS+METEO setup. We reported the overall eight days time series, and the comparison for the across site variability, the mean seasonal cycle and the eight days deviations (or anomalies) from the mean seasonal cycle.

Appendix C Median value of site-by-site performance per vegetation and climate type.

At follow we reported the median estimate of site-by-site R^2, RMSE, and absolute bias per PFT and climate zones.

Acknowledgments

G. Tramontana was supported by the GEOCARBON EU FP7 project (GA 283080). D. Papale, M. Jung and M. Reichstein thank the support of the BACI H2020 (GA 640176) EU project. G. Camps-Valls wants to acknowledge the support by an ERC Consolidator Grant with grant agreement 647423 (SEDAL). K. Ichii was supported by Environment Research and

Technology Development Funds (2-1401) from the Ministry of the Environment of Japan and the JAXA Global Change Observation Mission (GCOM) project (#115). C. R. Schwalm was supported by National Aeronautics and Space Administration (NASA) Grants #NNX12AP74G, #NNX10AG01A, and #NNX11AO08A. M. A. Arain thanks the support of Natural Sciences and Engineering Research Council (NSREC) of Canada. P. Serrano Ortiz was partially supported by the Spanish Ministry of Economy and Competitiveness though the project CGL2014-52838-C2-R(GEISpain). S. Wolf acknowledges support from a Marie Curie International Outgoing Fellowship (European Commission, grant 300083). This work used Eddy Covariance data acquired by the FLUXNET community and in particular by the following networks: AmeriFlux (U.S. Department of Energy, Biological and Environmental Research, Terrestrial Carbon Program (DE-FG02-04ER63917 and DE-FG02-04ER63911)), AfriFlux, AsiaFlux, CarboAfrica, CarboEuropeIP, CarboItaly, CarboMont,ChinaFlux, Fluxnet-Canada (supported by CFCAS, NSERC, BIOCAP, Environment Canada, and NRCan), GreenGrass, KoFlux, LBA, NECC, OzFlux, TCOS-Siberia, USCCC. We acknowledge the financial support to the eddy covariance data harmonization provided by CarboEuropeIP, FAO-GTOS-TCO, iLEAPS, Max Planck Institute for Biogeochemistry, National Science Foundation, University of Tuscia and US Department of Energy and the databasing and technical support from Berkeley Water Center, Lawrence Berkeley National Laboratory, Microsoft Research eScience, Oak Ridge National Laboratory, University of California - Berkeley, University of Virginia.

5. References

Amiro, B. D., Barr, A. G., Barr, J. G.,Black, T. A., Gracho, R., Brown, M., Chen, J., Clark, K. L., Davis, K. J., Desai, A. R., Dore, S., Engel, V., Fuentes, J. D., Goldstein, A. H., Goulden, M. L., Kolb, T. E., Lavigne, M. B., Law, B. E., Margolis, H. A., Martin, T., McCaughey, J. H., Misson, L., Montes, Helu, M., Noormets, A., Randerson, J. T., Starr, G. and Xiao, J.: Ecosystem carbon dioxide fluxes after disturbance in forests of North America. J Geophys Res-Biogeo, 115, G00K02, doi:10.1029/2010JG001390, 2010.

Alonso Fernández, J.R., DíazMuñiza, C., Garcia, Nieto, P.J., de Cos, Juez, F.J, Sánchez, Lasheras, F. and Roqueñíc, M.N.: Forecasting the cyanotoxins presence in fresh waters: A new model based on genetic algorithms combined with the MARS technique, Ecol Eng, 53, 68–78. doi:10.1016/j.ecoleng.2012.12.015, 2013.

Anav, A., Friedlingstein, P., Kidston, M., Bopp, L., Ciais, P., Cox, P., Jones, C., Jung, M., Myneni, R. and Zhu Z.: Evaluating the land and ocean components of the global carbon cycle in the cmip5 earth system models, J Climate, 26, 6801–6843, doi: http://dx.doi.org/10.1175/JCLI-D-12-00417.1, 2013.

Aubinet, M., Berbigier P., Bernhofer, CH. ., Cescatti, A., Feigenwinter, C., Granier, A., Grunwald, TH., Havrankova, K., Heinesch, B., Longdoz, B., Marcolla, B., Montagnani L., and P. Sedlak, P.: Comparing CO_2 storage and advenction conditions at night at different Carboeruroflux sites, Bound-lay meteorol, 116, 63–94, doi: 10.1007/s10546-004-7091-8, 2005.

Aubinet, M., Vesala, T. and Papale, D.: Eddy Covariance: A Practical Guide to Measurement and Data Analysis , Springer, Dordrecht Heidelberg London New York, 460, 2012.

Baldocchi, D.: Breathing of the terrestrial biosphere: lessons learned from a global network of carbon dioxide flux measurement systems, Aust J Bot, 56, 1–26, http://dx.doi.org/10.1071/BT07151, 2008.

Baldocchi, D.: Measuring fluxes of trace gases and energy between ecosystems and the atmosphere – the state and future of the eddy covariance method, Global Change Biol, 20, 3600-3609, DOI: 10.1111/gcb.12649, 2014.

Beer, C., Reichstein, M., Tomelleri, E., Ciais, P., Jung, M., Carvalhais, N., Rödenbeck, C., Arain, A., M., Baldocchi, D., Bonan, B., G., Bondeau, A., Cescatti, A., Lasslop, G., Lindroth, A., Lomas, M., Luyssaert, S., Margolis, H., Oleson, W. K., Roupsard, O., Veenendaal, E., Viovy, N., Woodward, I. F. and Papale, D.: Terrestrial Gross Carbon Dioxide Uptake: Global Distribution and Covariation with Climate, Science, 329, 834-838, doi: 10.1126/science.1184984, 2010.

Bell, T. W., Menzer, O., Troyo-Diéquez, E. and Oechel, W.: Carbon dioxide exchange over multiple temporal scales in an arid shrub ecosystem near La Paz, Baja California Sur, Mexico, Global Change Biol, 18, 2570–2582, doi:10.1111/j.1365-2486.2012.02720.x., 2012.

Bonan, G. B., Lawrence, P. J., Oleson, K. W., Levis, S., Jung, M., Reichstein, M., Lawrence, D. M. and Swenson, S. C.: Improving canopy processes in the Community Land Model version 4 (CLM4) using global flux fields empirically inferred from FLUXNET data, J Geophys Res-Biogeo, 116, G02014, doi:10.1029/2010JG001593, 2011.

Breiman, L.: Random Forests, Mach. Learn., 45 (1), 5–32, doi:10.1023/A:1010933404324, 2001.

Dee, D. P., Uppala, S. M., Simmons, A. J., Berrisford, P., Poli, P., Kobayashi, S., Andrae, U., Balmaseda, M. A., Balsamo, G., Bauer, P., Bechtold, P., Beljaars, A. C. M., van de Berg, L., Bidlot, J., Bormann, N., Delsol, C., Dragani, R., Fuentes, M., Geer, A. J., Haimberger, L., Healy, S. B., Hersbach, H., Hólm, E. V., Isaksen, L., Kållberg, P., Köhler, M., Matricardi, M., McNally, A. P., Monge-Sanz, B., M., Morcrette, J.-J., Park, B.-K., Peubey, C., de Rosnay, P., Tavolato, C., Thépaut, J.-N. and Vitart, F.: The ERA-Interim reanalysis: configuration and performance of the data assimilation system, Q.J.R. Meteorol Soc, 137, 553–597, doi: 10.1002/qj.828, 2011.

Frank, D., Reichstein, M., Bahn, M., Thonicke, K., Frank, D., Mahecha, M. D., Smith, P., Van Der Velde, M., Vicca, S., Babst, F., Beer, C., Buchmann, N., Canadell, J. G., Ciais, P., Cramer, W., Ibrom, A., Miglietta, F., Poulter, B., Ramming, A., Seneviratne, S. I., Walz, A., Wattenbach, M., Zavala, M. A. and Zscheischler, J.: Effects of climate extremes on the terrestrial carbon cycle: concepts, processes and potential future impacts, Global Change Biol, 21, 2861–2880, doi: 10.1111/gcb.12916, 2015.

Friedman, J. H.: Multivariate Adaptive Regression Splines, Ann. Statist., 19, 1-67, doi:10.1214/aos/1176347963, 1991.

Fröhlich, B., Rodner, E., Kemmler, M. and Denzler, J.: Large-scale gaussian process classification using random decision forests, S. Mach. Perc., 22 (1), 113–120, DOI 10.1007/s00138-012-0480-y, 2012.

Gao, B. C.: NDWI-A Normalized difference water index for remote sensing of vegetation liquid water from space, Remote Sens Environ, 58, 257-266, doi:10.1016/S0034-4257(96)00067-3, 1996.

Garnaud, C., Sushama, L. and Arorab, V. K.: The effect of driving climate data on the simulated terrestrial carbon pools and fluxes over North America, Int J Climatol, 34, 1098-1110, DOI: 10.1002/joc.3748, 2014.

Giri, C., Zhu, Z. and Reed B.: A comparative analysis of the Global Land Cover 2000 and MODIS land cover data sets, Remote Sens Environ, 94, 123–132, doi:10.1016/j.rse.2004.09.005, 2005

Gupta, H. V., Kling, H., Yilmaz, K. K. and Martinez, G. F.: Decomposition of the mean squared error and NSE performance criteria: Implications for improving hydrological modelling, J Hydrol, 20, 80-91, doi:10.1016/j.jhydrol.2009.08.003, 2009.

Hammerle, A., Haslwanter, A., Schmitt, M., Bahn, M., Tappeiner, U., Cernusca, A. and Wohlfahrt, G.: Eddy covariance measurements of carbon dioxide, latent and sensible energy fluxes above a meadow on a mountain slope. Bound-lay meteorol, 122(2), 397–416. http://doi.org/10.1007/s10546-006-9109-x, 2007

Haykin, S.: Neural Networks – A Comprehensive Foundation (2nd ed.)., Prentice Hall., 1999.

Ho, T. K.: The Random Subspace Method for Constructing Decision Forests, IEEE T Pattern Anal, 20 (8), 832–844, doi:10.1109/34.709601, 1998.

Huete, A., Didan, K., Miura, T., Rodriguez, E. P., Gao, X. and Ferreira, L.G.: Overview of the radiometric and biophysical performance of the MODIS vegetation indices, Remote Sens Environ, 83, 195–213, doi:10.1016/S0034-4257(02)00096-2, 2002.

Ichii, K., Wang, W., Hashimoto, H., Yang, F., Votava, P., Michaelis, A. R. and Nemani, R. R.: Refinement of rooting depths using satellite-based evapotranspiration seasonality for ecosystem modeling in California, Agr Forest Meteorol, 149, 1907-1918, doi:10.1016/j.agrformet.2009.06.019, 2009.

508 Ichii, K., Suzuki, T., Kato, T., Ito, A., Hajima, T., Ueyama, M., Sasai, T., Hirata, R., Saigusa, N., Ohtani, Y. and Takagi, K.:
509 Multi-model analysis of terrestrial carbon cycles in Japan: limitations and implications of model calibration using eddy flux
510 observations, Biogeosciences, 7, 2061–2080, doi:10.5194/bg-7-2061-2010, 2010.
511 IPCC: Climate Change 2007: Synthesis Report. Contribution of Working Groups I, II and III to the Fourth Assessment
512 Report of the Intergovernmental Panel on Climate Change [Core Writing Team, Pachauri, R.K and Reisinger, A. (eds.)].
513 IPCC, Geneva, Switzerland, 104, 2007.
514 Joiner, J., Yoshida, Y., Vasilkov, A. P., Schaefer, K., Jung, M., Guanter, L., Zhang, Y., Garrity, S., Middleton, E. M.,
515 Huemmrich, K. F., Guh, L. and Belelli Marchesini, L.: The seasonal cycle of satellite chlorophyll fluorescence observations
516 and its relationship to vegetation phenology and ecosystem atmosphere carbon exchange, Remote Sens Environ, 152, 375–
517 391, http://dx.doi.org/10.1016/j.rse.2014.06.022, 2014.
518 Jung, M., and Zscheischler, J.: A Guided Hybrid Genetic Algorithm for Feature Selection with Expensive Cost Functions,
519 Procedia Computer Science, 18, 2337-2346, doi: 10.1016/j.procs.2013.05.405, 2013.
520 Jung, M., Verstraete, M., Gobronz, N., Reichstein, M., Papale, D., Bondeau, A., Robustelli, M. and Pinty, R.: Diagnostic
521 assessment of European gross primary production, Global Change Biol, 14, 2349–2364, doi: 10.1111/j.1365-
522 2486.2008.01647.x, 2008.
523 Jung, M., Reichstein, M. and Bondeau, A.: Towards global empirical upscaling of FLUXNET Eddy Covariance
524 observations: validation of a model tree ensemble approach using a biosphere model, Biogeosciences, 6, 2001-2013,
525 doi:10.5194/bg-6-2001-2009, 2009.
526 Jung, M., Reichstein, M., Ciais, P., Seneviratne, S. I., Sheffield, J., Goulden, M. L., Bonan, G., Cescatti, A., Chen, J., de Jeu,
527 R., Dolman, A. J., Eugster, W., Gerten, D., Gianelle, D., Gobron, N., Heinke, J., Kimball, J., Law, B. E., Montagnani, L.,
528 Mu, Q., Mueller, B., Oleson, K., Papale, D., Richardson, A. D., Roupsard, O., Running, S., Tomelleri, E., Viovy, N., Weber,
529 U., Williams, C., Wood, E., Zaehle, S. and Zhang, K.: Recent decline in the global land evapotranspiration trend due to
530 limited moisture supply, Nature Letter, 467, 951-953, doi:10.1038/nature09396, 2010.
531 Jung, M., Reichstein, M., Margolis, H. A., Cescatti, A., Richardson, A. D., Arain, M. A., Arneth, A., Bernhofer, C., Bonal,
532 D., Chen, J., Gianelle, D., Gobron, N., Kiely, G., Kutsch, W., Lasslop, G., Law, B. E., Lindroth, A., Merbold, L.,
533 Montagnani, L., Moors, E. J., Papale, D., Sottocornola, M., Vaccari, F. and Williams, C.: Global patterns of land-atmosphere
534 fluxes of carbon dioxide, latent heat, and sensible heat derived from eddy covariance, satellite, and meteorological
535 observations, Journal of geophys res-Biogeo, 116, G00J07, doi:10.1029/2010JG001566, 2011.
536 Justice, C. O., Townshend, J. R. G., Vermote, E. F., Masuoka, E., Wolfe, R. E., Saleous, N., Roy, D. P. and Morisette, J. T.:
537 An overview of MODIS Land data processing and product status, Remote Sens Environ, 83, 3–15, doi:10.1016/S0034-
538 4257(02)00084-6, 2002.
539 Kondo, M., Ichii, K., Takagi, H. and Sasakawa, M.: Comparison of the data-driven top-down and bottom-up global
540 terrestrial CO2 exchanges: GOSAT CO2 inversion and empirical eddy flux upscaling, Journal of geophys res-Biogeo, 120,
541 1226–1245, doi:10.1002/2014JG002866, 2015.
542 Lasslop, G., Reichstein, M., Papale, D., Richardson, A. D., Arneth, A., Barr, A., Stoy, P. and Wohlfahrt, G.: Separation of
543 net ecosystem exchange into assimilation and respiration using a light response curve approach: critical issues and global
544 evaluation, Global Change Biol, 16, 187-208, doi:10.1111/j.1365-2486.2009.02041.x, 2010.
545 Merbold, L., Ardö, J., Arneth, A., Scholes, R. J., Nouvellon, Y., de Grandcourt, A., Archibald, S., Bonnefond, J. M.,
546 Boulain, N., Brueggemann, N., Bruemmer, C., Cappelaere, B., Ceschia, E., El-Khidir, H. A. M., El-Tahir, B. A., Falk, U.,
547 Lloyd, J., Kergoat, L., Le Dantec, V., Mougin, E., Muchinda, M., Mukelabai, M. M., Ramier, D., Roupsard, O., Timouk, F.,
548 Veenendaal,E. M. and Kutsch, W. L.: Precipitation as driver of carbon fluxes in 11 African ecosystems, Biogeosciences, 6,
549 1027–1041, doi:10.5194/bg-6-1027-2009, 2009, 2009.

Myneni, R.B., Hoffman, S., Knyazikhin, Y., Privette, J.L., Glassy, J., Tian, Y., Wang, Y., Song, X., Zhang, Y., Smith, G.R., Lotsch, A., Friedl, M., Morisette, J.T., Votava, P., Nemani, R.R., and Running, S.W.: Global products of vegetation leaf area and fraction absorbed PAR from year one of MODIS data, Remote Sens Environ, 83, 214–231, doi:10.1016/S0034-4257(02)00074-3, 2002.

Nash, J. E. and Sutcliffe J. V.: River flow forecasting through conceptual models part I: A discussion of principles, Journal Hydrol, 10, 282–290, doi:10.1016/0022-1694(70)90255-6, 1970.

Papale, D. and Valentini, R.: A new assessment of European forests carbon exchanges by eddy fluxes and artificial neural network spatialization, Global Change Biol, 9, 525–535, doi: 10.1046/j.1365-2486.2003.00609.x, 2003.

Papale, D., Reichstein, M., Aubinet, M., Canfora, E., Bernhofer, C., Kutsch, W., Longdoz, B., Rambal, S., Valentini, R., Vesala, T. and Yakir, D.: Towards a standardized processing of Net Ecosystem Exchange measured with eddy covariance technique: Algorithms and uncertainty estimation, Biogeosciences, 3, 571–583, doi:10.5194/bg-3-571-2006, 2006.

Papale, D., Black, T. A., Carvalhais, N., Cescatti, A., Chen, J., Jung, M., Kiely, G., Lasslop, G., Mahecha, D. M., Margolis, H., Merbold, L., Montagnani, L., Moors, E., Olesen, J. E., Reichstein, M., Tramontana, G., van Gorsel, E., Wohlfahrt, G. and Ráduly, B.: Effect of spatial sampling from European flux towers for estimating carbon and water fluxes with artificial neural networks, Journal of geophys res-Biogeo, 120, 1941-1957,doi: 10.1002/2015JG00299, 2015.

Paruelo, J. M., Piñero, G., Oyonarte, C., Alcaraz, D., Cabello, J. and Escribano, P.: Temporal and spatial patterns of ecosystem functioning in protected arid areas in southeastern Spain, Appl Veg Sci, 8, 93–102, doi: http://dx.doi.org/10.1658/1402-2001(2005)008[0093:TASPOE]2.0.CO;2, 2005.

Piao, S., Sitch, S., Ciais, P., Friedlingstein, P., Peylin, P., Wang, X., Ahlström, A., Anav, A., Canadell, J. G., Cong, N., Huntingford, C., Jung, M., Levis, S., Levy, P. E., Li, J., Lin, X., Lomas, M. R., Lu, M., Luo, Y., Ma, Y., Myneni, R. B., Poulter, B., Sun, Z., Wang, T., Viovy, N., Zaehle, S. and Zeng, N.: Evaluation of terrestrial carbon cycle models for their response to climate variability and to CO2 trends, Glob Change Biol., 19, 2117–2132, doi:10.1111/gcb.12187, 2013.

Rasmussen C. E. and Williams C. K. I.: Gaussian Processes for Machine Learning, the MIT Press, ISBN 026218253X, 2006.

Reichstein, M., Falge, E., Baldocchi, D., Papale, D., Aubinet, M., Berbigier, P., Bernhofer, C., Buchmann, N., Gilmanov, T., Granier, A., Grünwald, T., Havránková, K., Ilvesniemi, H., Janous, D., Knohl, A., Laurila, T., Lohila, A., Loustau, D., Matteucci, G., Meyers, T., Miglietta, F., Ourcival, J.-M., Pumpanen, J., Rambal, S., Rotenberg, E., Sanz, M., Tenhunen, J., Seufert, G., Vaccari, F., Vesala, T., Yakir, D., and Valentini R.: On the separation of net ecosystem exchange into assimilation and ecosystem respiration: Review and improved algorithm, Global Change Biol, 11, 1424–1439, doi:10.1111/j.1365-2486.2005.001002.x, 2005.

Reich, P. B.: The carbon dioxide exchange, Science, 329, 774-775, http://dx.doi.org/10.1126/science.1194353, 2010.

Schwalm C. R., Williams C. A., Schaefer K., Anderson R., Arain M. A., Baker I., Barr A., Black T. A., Chen G., Chen J. M., Ciais P., Davis K. J., Desai A., Dietze M., Dragoni D., Fischer M. L., Flanagan L. B., Grant R., Gu L., Hollinger D., Izaurralde R. C., Kucharik C., Lafleur P., Law B. E., Li L., Li Z., Liu S., Lokupitiya E., Luo Y., Ma S., Margolis H., Matamala R., McCaughey H., Monson R. K., Oechel W. C., Peng C., Poulter B., Price D. T., Riciutto D. M., Riley W., Sahoo A. K., Sprintsin M., Sun J., TI. H., Tonitto C., Verbeeck H., Verma S. B.: A model-data intercomparison of CO2 exchange across North America: Results from the North American Carbon Program site synthesis, Journal of geophys res-Biogeo, 115, G00H05, doi:10.1029/2009JG001229, 2010.

Schaaf, C. B., Gao, F., Strahler, A. H., Lucht, W., Li, X., Tsang, T., Strugnell, N. C., Zhang, X., Jin, Y., Muller, J-P., Lewis, P., Barnsley, M., Hobson, P., Disney, M., Roberts, G., Dunderdale, M., Doll, C., d'Entremont, R. P., Hu, B., Liang, S., Privette, J. L. and Roy, D.: First operational BRDF, albedo nadir reflectance products from MODIS, Remote Sens Environ, 83, 135–148, doi:10.1016/S0034-4257(02)00091-3, 2002.

Shawe-Taylor, J. and Cristianini, N.: Kernel Methods for Pattern Analysis, Cambridge University Press, 2004.

592 Shirmohammadi, R., Ghorbani, B., Hamedi, M., Hamedi, M. H., and Romeo, L. M.: Optimization of mixed refrigerant
593 systems in low temperature applications by means of group method of data handling (GMDH), Journal of Natural Gas
594 Science and Engineering, 26, 303-312, doi:10.1016/j.jngse.2015.06.028, 2015.
595 Sims, D. A., Rahman, A. F., Cordova, V. D., El-Masri, B. Z., Baldocchi, D. D., Bolstad, P. V., Flanagan, L. B., Goldstein, A.
596 H., Hollinger, D. Y., Misson, L., Monson, R. K., Oechel, W. C., Schmid, H. P., Wofsy, S. C. and Xu, L.: A new model of
597 gross primary productivity for North American ecosystems based solely on the enhanced vegetation index and land surface
598 temperature from MODIS, Remote Sens Environ, 12, 1633–1646, doi:10.1016/j.rse.2007.08.004, 2008.
599 Thornton, P. E., Law, B. E., Gholz, H. L., Clark, K. L., Falge, E., Ellsworth, D. S., Goldstein, A. H., Monson, R. K.,
600 Hollinger, D., Falk, M., Chen, J., Sparks, J. P.: Modeling and measuring the effects of disturbance history and climate on
601 carbon and water budgets in evergreen needleleaf forests, Agr Forest Meteorol, 113, 185-222, doi:10.1016/S0168-
602 1923(02)00108-9, 2002.
603 Tramontana, G., Ichii, K., Camps-Valls, G., Tomelleri, E. and Papale, D.: Uncertainty analysis of gross primary production
604 upscaling using Random Forests, remote sensing and eddy covariance data, Remote Sens Environ, 168, 360–373,
605 doi:10.1016/j.rse.2015.07.015, 2015.
606 Ungaro, F., Calzolari, C. and Busoni, E: Development of pedotransfer functions using a group method of data handling for
607 the soil of the Pianura Padano–Veneta region of North Italy: water retention properties, Geoderma, 124, 293–317,
608 doi:10.1016/j.geoderma.2004.05.007, 2005.
609 Valentini, R., Arneth, A., Bombelli, A., Castaldi, S., Cazzolla Gatti, R., Chevallier, F., Ciais, P., Grieco, E., Hartmann, J.,
610 Henry, M., Houghton, R. A., Jung, M., Kutsch, W. L., Malhi, Y., Mayorga, E., Merbold, L., Murray-Tortarolo, G., Papale,
611 D., Peylin, P., Poulter, B., Raymond, P. A., Santini, M., Sitch, S., Vaglio Laurin, G., van der Werf, G. R., Williams, C. A.
612 and Scholes, R. J.: A full greenhouse gases budget of Africa: synthesis, uncertainties, and vulnerabilities, Biogeosciences,
613 11, 381-407, doi:10.5194/bg-11-381-2014., 2014.
614 Vapnik, V., Golowich, S. and Smola, A.: Support vector method for function approximation, regression estimation, and
615 signal processing, Adv Neur In, 9, 281–287, 1997.
616 Verrelst, J., Muñoz, J., Alonso, L., Delegido, J., Rivera, J., Camps-Valls, G., and Moreno, J.: Machine learning regression
617 algorithms for biophysical parameter retrieval: Opportunities for Sentinel-2 and -3, Remote Sens Environ, 118, 127–139,
618 2012
619 Verrelst, J., Camps-Valls, G., Muñoz, J., Rivera, J. P., Veroustraete, F., Clevers, J. P. G. W. and Moreno, J.: Optical remote
620 sensing and the retrieval of terrestrial vegetation bio-geophysical properties – A review, ISPRS J Photogramm,
621 doi:10.1016/j.isprsjprs.2015.05.005, 108, 273-290, 2015
622 Wan, Z., Zhang, Y., Zhang, Q. and Li, Z. L.: Validation of the land-surface temperature products retrieved from Terra
623 Moderate Resolution Imaging Spectroradiometer data, Remote Sens Environ, 83, 163−180, doi: 10.1016/S0034-
624 4257(02)00093-7, 2002.
625 Wolf, S., Eugster, W., Potvin, C. and Buchmann, N.: Strong seasonal variations in net ecosystem CO2 exchange of a tropical
626 pasture and afforestation in Panama, Agr Forest Meteorol, 151, 1139-1151, doi:10.1016/j.agrformet.2011.04.002, 2011.
627 Xiao, J., Zhuang, Q., Baldocchi, D. D., Law, B. E., Richardson, A. D., Chen, J., Oren, R., Starr, G., Noormets, A., Ma, S.,
628 Verma, S. B., Wharton, S., Wofsy, S. C., Bolstad, P. V., Burns, S. P., Cook, D. R., Curtis, P. S., Drake, B. G., Falk, M.,
629 Fischer, M. L., Foster, D. R., Gu, L., Hadley, J. L., Hollinger, D. Y., Katul, G. G., Litvak, M., Martin, T. A., Matamala, R.,
630 McNulty, S., Meyers, T. P., Monson, R. K., Munger, J. W., Oechel, W. C., Paw U, K. T., Schmid, H. P., Scott, R. L., Sun,
631 G., Suyker, A. E., Torn, M. S.: Estimation of net ecosystem carbon exchange for the conterminous United States by
632 combining MODIS and AmeriFlux data, Agr Forest Meteorol, 148, 1827-1847, doi:10.1016/j.agrformet.2008.06.015, 2008.
633 Xiao, J., Zhuang, Q., Law, B. E., Chen, J., Baldocchi, D. D., Cook, D. R., Oren, R., Richardson, A. D., Wharton, S., Ma, S.,
634 Martin, T. A., Verma, S. B., Suyker, A. E., Scott, R. L., Monson, R. K., Litvak, M., Hollinger, D. Y., Sun, G., Davis, K. J.,

635 Bolstad, P. V., Burns, S. P., Curtis, P. S., Drake, B. G., Falk, M., Fischer, M. L., Foster, D. R., Gu, L., Hadley, J. L., Katul,
636 G. G., Matamala, R., McNulty, S., Meyers, T., P., Munger, J. W., Noormets, A., Oechel, W. C., Paw, K. T., Schmid, H. P.,
637 Starr, G. Torn, M. S. and Wofsy, S. C.: A continuous measure of gross primary production for the conterminous United
638 States derived from MODIS and AmeriFlux data, Remote Sens Environ, 114, 576–591, doi: 10.1016/j.rse.2009.10.013,
639 2010.
640 Xiao, X., Boles, S., Liu, J. Y., Zhuang, D. F. and Liu, M. L.: Characterization of forest types in Northeastern China, using
641 multi-temporal SPOT-4 VEGETATION sensor data, Remote Sens Environ, 82, 335–348, doi:10.1016/S0034-
642 4257(02)00051-2, 2002.
643 Yang, F., White, M. A., Michaelis, A. R., Ichii, K., Hashimoto, H., Votava, P., Zhu, A. X. and Nemani, R. R.: Prediction of
644 continental-scale evapotranspiration by combining MODIS and AmeriFlux data through support Vector machine, IEEE T.
645 Geosci Remote, 44, 3452-3461, doi: 10.1109/TGRS.2006.876297, 2006.
646 Yang, F., Ichii, K., White, M. A., Hashimoto, H., Michaelis, A. R., Votava, P., Zhu, A-X., Huete, A., Running, S. W., and
647 Nemani, R. R.: Developing a continental-scale measure of gross primary production by combining MODIS and AmeriFlux
648 data through Support Vector Machine approach, Remote Sens Environ, 110, 109–122, doi:10.1016/j.rse.2007.02.016, 2007.
649 Yebra, M., Van Dijk, A. I. J. M., Leuning, R. and Guerschman, J. P.: Global vegetation gross primary production estimation
650 using satellite-derived light-use efficiency and canopy conductance, Remote Sens Environ, 163, 206–216,
651 doi:10.1016/j.rse.2015.03.016, 2015.
652 Yuan, W., Liu, S., Yu, G., Bonnefond, J-M., Chen, J., Davis, K., Desai, A. R., Goldstein, A. H., Gianelle, D., Rossi, F.,
653 Suyker, A. E. and Verma, S. B.: Global estimates of evapotranspiration and gross primary production based on MODIS and
654 global meteorology data, Remote Sens Environ, 114, 1416–1431, doi:10.1016/j.rse.2010.01.022, 2010.
655 Zhao, Y., Ciais, P., Pylin, P., Viovy, N., Longdoz, B., Bonnefond, J. M., Rambal, S., Klumpp, K., Olioso, A., Cellier, P.,
656 Maigna, F., Eglin, T. and Calvet, J. C.: How errors on meteorological variables impact simulated ecosystem fluxes: a case
657 study for six French sites, Biogeosciences, 9, 2537-2564, doi:10.5194/bg-9-2537-2012, 2012.

Biogeosciences Discuss., doi:10.5194/bg-2015-661, 2016
Manuscript under review for journal Biogeosciences
Published: 7 March 2016

658 **Table 1.** Distribution of flux tower sites across plant functional types (PFT) and climate zones.

PFT	N° of sites	Climate zone	N° of sites
Evergreen needleleaf forest	66	Temperate	111
Grassland	38	Subtropical - Mediterranean	47
Cropland	27	Boreal	34
Deciduous broadleaf forest	24	Tropical	14
Evergreen broadleaf forest	19	Dry	13
Wetland	17	Artic	5
Shrubland	12		
Mixed forest	11		
Savannah	10		

Biogeosciences Discuss., doi:10.5194/bg-2015-661, 2016
Manuscript under review for journal Biogeosciences
Published: 7 March 2016

Table 2. Selected predictors for both setup for CO_2 fluxes (GPP, TER and NEE) and energy fluxes (H, LE and Rn). List of acronyms: Enhanced Vegetation Index (EVI), fraction of photosynthetically active radiation absorbed by a canopy (fPAR), Leaf Area Index (LAI), daytime Land Surface Temperature (LST_{Day}) and nighttime Land Surface Temperature (LST_{Night}), Middle Infrared Reflectance (band 7) (MIR[(1)]), Normalized Difference Vegetation Index (NDVI), Normalized Difference Water Index (NDWI), Plant Functional Type (PFT), incoming global Radiation (Rg), top of atmosphere potential Radiation (Rpot), Index of Water Availability (IWA), Relative humidity (Rh), Water Availability Index lower (WAI_L), and upper (WAI_U) (for details see supplementary material, Sect. S3), Mean Seasonal Cycle (MSC). Interaction between A and B is shown as (A, B)

Setup	Type of variability	CO_2 fluxes	Energy fluxes
RS	Spatial	PFT	PFT
		Amplitude of MSC of EVI	Maximum of MSC of (fPAR, Rg)
		Amplitude of MSC of MIR[(1)]	Minimum of MSC of (NDVI, Rg)
		Maximum of MSC of LST_{Day}	
	Spatial & seasonal	MSC LAI	MSC of (EVI, LST)
			Rpot
	Spatial, seasonal & interannual	NDWI	Rg
		LST_{Day}	LST_{Day}
		LST_{Night}	Anomalies of LST_{Night}
		(NDVI, Rg)	Anomalies of (EVI, LST)
RS+METEO	Spatial	PFT	PFT
		Amplitude of MSC of NDVI	Maximum of MSC of (NDVI, WAI_U)
		Amplitude of MSC of band 4 BRDF reflectance[(2)]	Mean of MSC of band 6 BRDF reflectance[(2)]
		Minimum of MSC of NDWI	
		Amplitude of MSC of (NDVI, WAI_L)	
	Spatial & Seasonal	MSC of LST_{Night}	Rpot
		MSC of (FPAR, LST)	MSC of NDWI
		MSC of (NDVI, Rg)	MSC of LST_{Night}
			MSC of (NDVI, Rg, IWA)
	Spatial & Seasonal & Interannual	Tair	Rain
			Rg
			Rh

[(1)] derived from the MOD13 product; [(2)] derived from MCD43 product.

Biogeosciences Discuss., doi:10.5194/bg-2015-661, 2016
Manuscript under review for journal Biogeosciences
Published: 7 March 2016

667 **Table** 3. Statistics of the accuracy of predictions of CO_2 and energy fluxes made by the ensemble median estimate based on RS and
668 RS+METEO. For RMSE and BIAS, the reference units were $gCm^{-2}d^{-1}$ and $MJm^{-2}d^{-1}$, in the case of CO_2 fluxes (GPP, TER and NEE) and
669 energy fluxes (H, LE and Rn) respectively.

Flux	RS					RS+METEO				
	MEF	RMSE	P	ROV	BIAS	MEF	RMSE	ρ	ROV	BIAS
GPP_R	0.71	1.56	0.85	0.69	-0.02	0.70	1.59	0.84	0.73	0.09
GPP_L	0.71	1.53	0.84	0.68	-0.02	0.71	1.54	0.84	0.74	0.09
TER_R	0.64	1.14	0.80	0.61	-0.01	0.64	1.15	0.80	0.69	0.09
TER_L	0.60	1.18	0.77	0.56	-0.01	0.63	1.14	0.79	0.66	0.08
NEE	0.46	1.24	0.68	0.39	0.04	0.43	1.28	0.65	0.40	-0.02
H	0.79	1.36	0.89	0.71	-0.02	0.79	1.37	0.89	0.75	0.02
LE	0.76	1.37	0.87	0.71	-0.07	0.75	1.39	0.87	0.73	-0.01
Rn	0.92	1.51	0.96	0.90	-0.01	0.91	1.55	0.96	0.93	0.08

670

Biogeosciences Discuss., doi:10.5194/bg-2015-661, 2016
Manuscript under review for journal Biogeosciences
Published: 7 March 2016

671 **Table 4**: Mean values of the determination coefficient (R^2) by the pair-wise comparison of the models output and their residuals. We
672 compared different ML and same drivers (RS and RS+METEO respectively) or the same ML and different drivers (RS vs
673 RS+METEO). Numbers in brackets were the standard deviation of R^2. All correlations were statistically significant ($p < 0.001$).

Fluxes	Correlation among models output			Correlation among models residuals		
	RS	RS+METEO	RS vs RS+METEO	RS	RS+METEO	RS vs RS+METEO
GPP_R	0.95 (0.02)	0.95 (0.02)	0.89 (0.02)	0.88 (0.04)	0.87 (0.04)	0.74 (0.04)
GPP_L	0.95 (0.02)	0.94 (0.02)	0.88 (0.02)	0.88 (0.04)	0.86 (0.04)	0.72 (0.04)
TER_R	0.91 (0.03)	0.94 (0.03)	0.86 (0.04)	0.86 (0.05)	0.88 (0.05)	0.75 (0.06)
TER_L	0.92 (0.03)	0.93 (0.03)	0.85 (0.03)	0.89 (0.04)	0.88 (0.05)	0.77 (0.05)
NEE	0.84 (0.06)	0.84 (0.07)	0.75 (0.08)	0.88 (0.05)	0.87 (0.06)	0.80 (0.06)
H	0.94 (0.02)	0.96 (0.02)	0.93 (0.03)	0.80 (0.06)	0.87 (0.05)	0.76 (0.08)
LE	0.94 (0.02)	0.96 (0.01)	0.90 (0.02)	0.83 (0.05)	0.88 (0.04)	0.73 (0.04)
Rn	0.98 (0.01)	0.99 (0.00)	0.97 (0.01)	0.79 (0.08)	0.86 (0.03)	0.71 (0.12)

674

Biogeosciences Discuss., doi:10.5194/bg-2015-661, 2016
Manuscript under review for journal Biogeosciences
Published: 7 March 2016

675 **Table 5**: R^2 and RMSE for the comparison among sites, mean seasonal cycle and anomalies. The last two columns showed the consistency
676 between the median estimates of the two setups. For RMSE, the reference units were $gCm^{-2}d^{-1}$ and $MJm^{-2}d^{-1}$, in the case of CO_2 fluxes
677 (GPP, TER and NEE) and energy fluxes (H, LE and Rn) respectively.

Fluxes	RS *vs.* OBS		RS+METEO *vs.* OBS		RS *vs.* RS+METEO	
	R^2	RMSE	R^2	RMSE	R^2	RMSE
Across-sites						
GPP_R	0.78	0.80	0.77	0.82	0.95	0.34
GPP_L	0.78	0.77	0.79	0.75	0.94	0.36
TER_R	0.68	0.73	0.61	0.81	0.92	0.32
TER_L	0.72	0.60	0.71	0.61	0.92	0.27
NEE	0.48	0.61	0.46	0.61	0.83	0.22
H	0.81	0.68	0.81	0.68	0.97	0.25
LE	0.79	0.74	0.75	0.80	0.93	0.33
Rn	0.80	0.93	0.79	0.96	0.96	0.38
Mean Seasonal Cycle						
GPP_R	0.76	1.03	0.77	1.02	0.93	0.48
GPP_L	0.77	1.00	0.77	0.99	0.93	0.50
TER_R	0.71	0.62	0.71	0.62	0.92	0.29
TER_L	0.67	0.64	0.68	0.63	0.92	0.29
NEE	0.61	0.83	0.59	0.84	0.93	0.24
H	0.86	0.89	0.86	0.87	0.97	0.36
LE	0.87	0.79	0.87	0.79	0.95	0.45
Rn	0.98	0.74	0.98	0.74	0.99	0.43
Anomalies						
GPP_R	0.18	0.67	0.12	0.68	0.38	0.32
GPP_L	0.16	0.67	0.11	0.68	0.37	0.31
TER_R	0.14	0.48	0.15	0.48	0.36	0.17
TER_L	0.10	0.58	0.13	0.57	0.35	0.18
NEE	0.13	0.56	0.13	0.55	0.43	0.20
H	0.43	0.81	0.41	0.81	0.77	0.34
LE	0.21	0.78	0.21	0.77	0.46	0.32
Rn	0.57	0.81	0.54	0.83	0.84	0.41

678

Biogeosciences Discuss., doi:10.5194/bg-2015-661, 2016
Manuscript under review for journal Biogeosciences
Published: 7 March 2016

679 **Table A1**: Accuracy of CO_2 and energy fluxes predicted by machine learning methods based on RS and RS+METEO dataset. The median
680 value of methods and the variability (in brackets) estimated as the median absolute deviation (MAD) from the median multiplied per
681 1.4826 (as reported in Jung et al., 2009) were reported.

FLUXES	RS			RS+METEO		
	MEF	RMSE	Abs BIAS	MEF	RMSE	Abs BIAS
GPP	0.698 (±0.012)	1.604 (±0.033)	0.022 (±0.019)	0.694 (±0.012)	1.614 (±0.032)	0.073 (±0.011)
GPP_{HB}	0.700 (±0.009)	1.564 (±0.024)	0.023 (±0.024)	0.701 (±0.008)	1.561 (±0.020)	0.083 (±0.011)
TER	0.612 (±0.022)	1.183 (±0.033)	0.026 (±0.025)	0.623 (±0.005)	1.166 (±0.008)	0.089 (±0.033)
TER_{HB}	0.571 (±0.016)	1.218 (±0.023)	0.019 (±0.017)	0.609 (±0.001)	1.163 (±0.002)	0.079 (±0.017)
NEE	0.433 (±0.017)	1.270 (±0.019)	0.024 (±0.021)	0.407 (±0.029)	1.298 (±0.032)	0.014 (±0.003)
H	0.767 (±0.015)	1.426 (±0.047)	0.014 (±0.005)	0.776 (±0.008)	1.397 (±0.025)	0.022 (±0.009)
LE	0.739 (±0.015)	1.418 (±0.042)	0.052 (±0.046)	0.734 (±0.003)	1.434 (±0.009)	0.023 (±0.008)
Rn	0.909 (±0.009)	1.589 (±0.082)	0.030 (±0.025)	0.908 (±0.008)	1.600 (±0.070)	0.073 (±0.015)

682

Biogeosciences Discuss., doi:10.5194/bg-2015-661, 2016
Manuscript under review for journal Biogeosciences
Published: 7 March 2016

Biogeosciences
Discussions
Open Access
EGU

683
684
685

Table C1. Median site-by-site R^2 of the CO_2 fluxes per PFT and climate zones. ENF was evergreen needle leaf forest, DBF deciduous broadleaf forest, EBF Evergreen broadleaf forest, MF mixed forest, SHR shrubland, SAV Savannah, GRA Grassland, CRO cropland, WET Wetland, Trop Tropical, SubTrop Subtropical, Dry Dryland, Tmp Temperate, TmpCont Temperate-continental, Bor Boreal, Cold cold environment or Iceland covered by ice.

CAT	GPP_R		GPP_L		TER_R		TER_L		NEE	
	RS	RS+METEO	RS	RS+METEO	RS	RS+METEO	RS	RS+METEO	RS	RS+METEO
ENF	0.87 (0.10)	0.86 (0.10)	0.85 (0.12)	0.86 (0.12)	0.81 (0.15)	0.85 (0.11)	0.75 (0.24)	0.76 (0.20)	0.50 (0.34)	0.55 (0.30)
DBF	0.89 (0.07)	0.87 (0.09)	0.87 (0.07)	0.88 (0.08)	0.81 (0.12)	0.83 (0.13)	0.76 (0.14)	0.76 (0.14)	0.72 (0.16)	0.68 (0.17)
EBF	0.50 (0.29)	0.48 (0.20)	0.48 (0.29)	0.44 (0.28)	0.34 (0.34)	0.49 (0.35)	0.15 (0.18)	0.29 (0.20)	0.26 (0.23)	0.24 (0.26)
MF	0.91 (0.06)	0.95 (0.02)	0.91 (0.03)	0.95 (0.04)	0.85 (0.10)	0.90 (0.07)	0.84 (0.10)	0.86 (0.15)	0.73 (0.10)	0.75 (0.09)
SHR	0.67 (0.30)	0.71 (0.28)	0.67 (0.36)	0.72 (0.23)	0.80 (0.13)	0.78 (0.24)	0.68 (0.18)	0.66 (0.38)	0.37 (0.38)	0.41 (0.31)
SAV	0.75 (0.13)	0.70 (0.13)	0.72 (0.05)	0.67 (0.17)	0.65 (0.07)	0.72 (0.11)	0.55 (0.16)	0.61 (0.10)	0.38 (0.20)	0.34 (0.29)
GRA	0.69 (0.27)	0.62 (0.33)	0.69 (0.25)	0.60 (0.32)	0.70 (0.25)	0.73 (0.25)	0.66 (0.20)	0.72 (0.21)	0.40 (0.29)	0.36 (0.30)
CRO	0.58 (0.41)	0.44 (0.36)	0.56 (0.41)	0.45 (0.31)	0.78 (0.17)	0.76 (0.15)	0.68 (0.22)	0.65 (0.23)	0.35 (0.46)	0.33 (0.43)
WET	0.87 (0.11)	0.91 (0.07)	0.85 (0.12)	0.87 (0.09)	0.78 (0.19)	0.83 (0.14)	0.65 (0.17)	0.74 (0.20)	0.64 (0.16)	0.61 (0.24)
Trop	0.32 (0.46)	0.40 (0.39)	0.63 (0.23)	0.31 (0.32)	0.25 (0.23)	0.34 (0.47)	0.11 (0.13)	0.26 (0.14)	0.28 (0.35)	0.21 (0.30)
SubTrop	0.64 (0.26)	0.66 (0.28)	0.65 (0.26)	0.65 (0.24)	0.64 (0.25)	0.66 (0.26)	0.52 (0.24)	0.55 (0.28)	0.39 (0.37)	0.39 (0.26)
Dry	0.47 (0.27)	0.40 (0.33)	0.50 (0.25)	0.38 (0.30)	0.62 (0.25)	0.62 (0.38)	0.55 (0.19)	0.55 (0.39)	0.21 (0.29)	0.11 (0.14)
Tmp	0.81 (0.19)	0.74 (0.24)	0.83 (0.14)	0.78 (0.22)	0.78 (0.13)	0.77 (0.18)	0.68 (0.20)	0.72 (0.17)	0.56 (0.28)	0.47 (0.34)
TmpCont	0.86 (0.09)	0.82 (0.16)	0.84 (0.11)	0.80 (0.17)	0.81 (0.12)	0.78 (0.14)	0.75 (0.17)	0.76 (0.15)	0.54 (0.42)	0.53 (0.36)
Bor	0.90 (0.07)	0.90 (0.07)	0.92 (0.06)	0.89 (0.07)	0.90 (0.05)	0.91 (0.04)	0.86 (0.08)	0.89 (0.06)	0.59 (0.31)	0.59 (0.25)
Cold	0.56 (0.57)	0.50 (0.56)	0.49 (0.62)	0.46 (0.59)	0.84 (0.20)	0.86 (0.13)	0.50 (0.38)	0.55 (0.23)	0.47 (0.56)	0.45 (0.57)

Biogeosciences Discuss., doi:10.5194/bg-2015-661, 2016
Manuscript under review for journal Biogeosciences
Published: 7 March 2016

Biogeosciences
Discussions
Open Access
EGU

686
687
688

Table C2. Median site-by-site RMSE of the CO_2 fluxes per PFT and climate zones. ENF was svergreen needle leaf forest, DBF deciduous broadleaf forest, EBF Evergreen broadleaf forest, MF mixed forest, SHR shrubland, SAV Savannah, GRA Grassland, CRO cropland, WET Wetland, Trop Tropical, SubTrop Subtropical, Dry Dryland, Tmp Temperate, TmpCont Temperate-continental, Bor Boreal, Cold cold environment or Iceland covered by ice.

CAT	GPP_R ($gCm^{-2}d^{-1}$)		GPP_L ($gCm^{-2}d^{-1}$)		TER_R ($gCm^{-2}d^{-1}$)		TER_L ($gCm^{-2}d^{-1}$)		NEE ($gCm^{-2}d^{-1}$)	
	RS	RS+METEO	RS	RS+METEO	RS	RS+METEO	RS	RS+METEO	RS	RS+METEO
ENF	1.05 (0.60)	1.12 (0.60)	1.04 (0.59)	1.14 (0.66)	0.82 (0.50)	0.80 (0.52)	0.87 (0.60)	0.91 (0.68)	0.87 (0.51)	0.86 (0.53)
DBF	1.21 (0.78)	1.35 (0.59)	1.17 (0.68)	1.36 (0.62)	0.68 (0.26)	0.76 (0.33)	0.76 (0.33)	0.93 (0.44)	1.28 (0.39)	1.28 (0.39)
EBF	1.70 (0.55)	1.64 (0.85)	1.65 (0.70)	1.46 (0.51)	1.23 (0.69)	1.48 (0.85)	1.88 (1.23)	1.71 (0.73)	1.15 (0.48)	1.15 (0.45)
MF	0.87 (0.17)	0.76 (0.45)	0.89 (0.27)	0.97 (0.56)	0.65 (0.18)	0.73 (0.42)	0.79 (0.14)	0.79 (0.18)	0.91 (0.47)	0.81 (0.29)
SHR	0.73 (0.47)	0.78 (0.46)	0.69 (0.44)	0.77 (0.37)	0.50 (0.33)	0.70 (0.41)	0.50 (0.34)	0.55 (0.36)	0.57 (0.31)	0.52 (0.15)
SAV	0.83 (0.44)	0.81 (0.18)	0.87 (0.45)	0.84 (0.18)	0.80 (0.53)	0.68 (0.41)	0.86 (0.55)	0.77 (0.38)	0.71 (0.36)	0.69 (0.31)
GRA	1.22 (0.64)	1.22 (0.60)	1.18 (0.68)	1.20 (0.62)	1.00 (0.48)	1.01 (0.54)	0.99 (0.58)	0.95 (0.52)	0.76 (0.61)	0.85 (0.49)
CRO	1.69 (1.38)	2.30 (1.02)	1.57 (1.42)	2.24 (1.10)	0.87 (0.46)	0.90 (0.57)	0.80 (0.51)	0.98 (0.57)	1.42 (0.90)	1.44 (0.70)
WET	1.04 (0.95)	0.93 (0.77)	1.03 (0.96)	0.78 (0.53)	1.04 (0.87)	0.98 (0.82)	1.07 (0.51)	1.02 (0.51)	0.46 (0.19)	0.64 (0.26)
Trop	1.93 (0.46)	1.74 (1.01)	2.24 (0.62)	1.56 (0.78)	2.07 (0.69)	1.55 (0.87)	2.47 (0.74)	2.05 (0.43)	1.28 (0.29)	1.17 (0.46)
SubTrop	1.37 (0.55)	1.40 (0.61)	1.37 (0.56)	1.38 (0.57)	1.03 (0.46)	1.00 (0.41)	1.08 (0.36)	1.11 (0.40)	1.13 (0.63)	1.15 (0.62)
Dry	0.60 (0.24)	0.78 (0.36)	0.63 (0.16)	0.74 (0.30)	0.49 (0.10)	0.54 (0.20)	0.58 (0.26)	0.67 (0.32)	0.41 (0.13)	0.46 (0.15)
Tmp	1.73 (1.02)	1.82 (0.99)	1.73 (0.98)	1.71 (1.03)	1.09 (0.54)	1.17 (0.67)	1.24 (0.57)	1.31 (0.59)	1.43 (0.59)	1.40 (0.61)
TmpCont	1.01 (0.42)	1.29 (0.59)	1.00 (0.45)	1.26 (0.57)	0.71 (0.30)	0.75 (0.38)	0.74 (0.31)	0.79 (0.34)	0.95 (0.39)	1.02 (0.43)
Bor	0.66 (0.27)	0.70 (0.36)	0.66 (0.27)	0.67 (0.33)	0.48 (0.27)	0.47 (0.27)	0.48 (0.16)	0.45 (0.21)	0.50 (0.32)	0.48 (0.22)
Cold	0.44 (0.04)	0.58 (0.42)	0.51 (0.24)	0.46 (0.32)	0.41 (0.06)	0.23 (0.06)	0.57 (0.16)	0.29 (0.12)	0.51 (0.21)	0.54 (0.35)

Biogeosciences Discuss., doi:10.5194/bg-2015-661, 2016
Manuscript under review for journal Biogeosciences
Published: 7 March 2016

Biogeosciences
Discussions
Open Access
EGU

689 **Table C3.** Median site-by-site absolute bias of the CO_2 fluxes per PFT and climate zones. ENF was evergreen needle leaf forest, DBF deciduous broadleaf forest, EBF Evergreen broadleaf forest, MF mixed
690 forest, SHR shrubland, SAV Savannah, GRA Grassland, CRO cropland, WET Wetland, Trop Tropical, SubTrop Subtropical, Dry Dryland, Tmp Temperate, TmpCont Temperate-continental, Bor Boreal,
691 Cold cold environment or Iceland covered by ice.

CAT	GPP_R ($gCm^{-2}d^{-1}$)		GPP_L ($gCm^{-2}d^{-1}$)		TER_R ($gCm^{-2}d^{-1}$)		TER_L ($gCm^{-2}d^{-1}$)		NEE ($gCm^{-2}d^{-1}$)	
	RS	RS+METEO	RS	RS+METEO	RS	RS+METEO	RS	RS+METEO	RS	RS+METEO
ENF	0.53 (0.46)	0.54 (0.56)	0.45 (0.42)	0.48 (0.50)	0.47 (0.47)	0.50 (0.54)	0.42 (0.40)	0.41 (0.43)	0.39 (0.44)	0.32 (0.36)
DBF	0.43 (0.38)	0.56 (0.59)	0.42 (0.36)	0.50 (0.52)	0.29 (0.32)	0.35 (0.35)	0.39 (0.33)	0.42 (0.34)	0.60 (0.28)	0.55 (0.30)
EBF	0.82 (0.91)	0.77 (0.50)	0.75 (0.81)	0.76 (0.48)	0.88 (0.98)	0.84 (0.72)	0.76 (0.81)	0.93 (0.65)	0.36 (0.45)	0.46 (0.44)
MF	0.47 (0.20)	0.34 (0.38)	0.38 (0.29)	0.57 (0.29)	0.39 (0.28)	0.41 (0.13)	0.37 (0.15)	0.30 (0.35)	0.34 (0.49)	0.32 (0.36)
SHR	0.38 (0.37)	0.54 (0.49)	0.38 (0.44)	0.39 (0.47)	0.36 (0.38)	0.50 (0.43)	0.31 (0.40)	0.32 (0.23)	0.27 (0.27)	0.28 (0.24)
SAV	0.42 (0.40)	0.36 (0.21)	0.35 (0.40)	0.23 (0.15)	0.43 (0.41)	0.35 (0.23)	0.42 (0.37)	0.31 (0.10)	0.23 (0.21)	0.19 (0.10)
GRA	0.60 (0.59)	0.48 (0.49)	0.60 (0.56)	0.52 (0.55)	0.38 (0.29)	0.36 (0.37)	0.44 (0.39)	0.38 (0.38)	0.17 (0.20)	0.31 (0.31)
CRO	0.47 (0.37)	0.66 (0.44)	0.36 (0.33)	0.56 (0.47)	0.29 (0.32)	0.25 (0.22)	0.29 (0.32)	0.30 (0.29)	0.41 (0.31)	0.56 (0.55)
WET	0.54 (0.64)	0.28 (0.41)	0.55 (0.62)	0.29 (0.25)	0.72 (0.35)	0.48 (0.52)	0.69 (0.29)	0.50 (0.51)	0.24 (0.19)	0.30 (0.25)
Trop	1.66 (1.31)	0.67 (0.79)	1.71 (1.23)	0.77 (0.86)	1.73 (0.88)	1.16 (1.19)	1.94 (0.81)	1.21 (0.67)	0.52 (0.57)	0.38 (0.55)
SubTrop	0.54 (0.45)	0.55 (0.43)	0.50 (0.38)	0.52 (0.55)	0.46 (0.44)	0.53 (0.47)	0.47 (0.35)	0.42 (0.37)	0.34 (0.44)	0.37 (0.34)
Dry	0.31 (0.20)	0.33 (0.26)	0.33 (0.38)	0.36 (0.29)	0.24 (0.21)	0.32 (0.35)	0.34 (0.21)	0.43 (0.26)	0.14 (0.08)	0.22 (0.14)
Tmp	0.72 (0.55)	0.77 (0.71)	0.66 (0.59)	0.63 (0.56)	0.50 (0.46)	0.47 (0.50)	0.51 (0.55)	0.41 (0.45)	0.46 (0.43)	0.51 (0.41)
TmpCont	0.45 (0.35)	0.60 (0.52)	0.39 (0.35)	0.57 (0.47)	0.37 (0.28)	0.29 (0.25)	0.37 (0.33)	0.38 (0.37)	0.35 (0.40)	0.55 (0.55)
Bor	0.36 (0.30)	0.32 (0.34)	0.32 (0.24)	0.27 (0.31)	0.32 (0.40)	0.32 (0.33)	0.31 (0.35)	0.26 (0.32)	0.27 (0.26)	0.23 (0.26)
Cold	0.07 (0.00)	0.08 (0.09)	0.08 (0.12)	0.15 (0.06)	0.34 (0.04)	0.12 (0.06)	0.34 (0.06)	0.15 (0.01)	0.37 (0.15)	0.27 (0.27)

Biogeosciences Discuss., doi:10.5194/bg-2015-661, 2016
Manuscript under review for journal Biogeosciences
Published: 7 March 2016

692 **Table C4.** Median site-by-site R^2 of the energy fluxes per PFT and climate zones. ENF was evergreen needle leaf forest, DBF deciduous
693 broadleaf forest, EBF Evergreen broadleaf forest, MF mixed forest, SHR shrubland, SAV Savannah, GRA Grassland, CRO cropland,
694 WET Wetland, Trop Tropical, SubTrop Subtropical, Dry Dryland, Tmp Temperate, TmpCont Temperate-continental, Bor Boreal, Cold
695 cold environment or Iceland covered by ice.

CAT	H		LE		Rn	
	RS	RS+METEO	RS	RS+METEO	RS	RS+METEO
ENF	0.87 (0.10)	0.86 (0.10)	0.83 (0.10)	0.84 (0.11)	0.97 (0.02)	0.97 (0.02)
DBF	0.76 (0.18)	0.74 (0.12)	0.87 (0.05)	0.87 (0.07)	0.97 (0.01)	0.97 (0.02)
EBF	0.85 (0.13)	0.82 (0.17)	0.56 (0.30)	0.52 (0.42)	0.95 (0.05)	0.96 (0.03)
MF	0.85 (0.06)	0.82 (0.10)	0.91 (0.07)	0.89 (0.06)	0.97 (0.02)	0.96 (0.02)
SHR	0.83 (0.15)	0.83 (0.17)	0.73 (0.29)	0.77 (0.23)	0.98 (0.01)	0.97 (0.01)
SAV	0.74 (0.25)	0.77 (0.26)	0.85 (0.06)	0.78 (0.11)	0.86 (0.05)	0.88 (0.10)
GRA	0.72 (0.22)	0.71 (0.22)	0.85 (0.11)	0.83 (0.16)	0.96 (0.02)	0.96 (0.02)
CRO	0.70 (0.16)	0.66 (0.18)	0.79 (0.14)	0.80 (0.14)	0.97 (0.02)	0.96 (0.02)
WET	0.81 (0.06)	0.78 (0.14)	0.86 (0.10)	0.84 (0.06)	0.94 (0.02)	0.92 (0.06)
Trop	0.52 (0.18)	0.60 (0.32)	0.56 (0.38)	0.50 (0.44)	0.86 (0.14)	0.89 (0.13)
SubTrop	0.81 (0.18)	0.82 (0.18)	0.78 (0.13)	0.80 (0.13)	0.96 (0.03)	0.96 (0.02)
Dry	0.87 (0.07)	0.86 (0.13)	0.80 (0.07)	0.79 (0.14)	0.90 (0.06)	0.93 (0.05)
Tmp	0.78 (0.14)	0.78 (0.13)	0.86 (0.11)	0.83 (0.13)	0.97 (0.02)	0.96 (0.02)
TmpCont	0.72 (0.18)	0.69 (0.18)	0.83 (0.08)	0.84 (0.09)	0.97 (0.02)	0.96 (0.02)
Bor	0.90 (0.07)	0.89 (0.08)	0.92 (0.05)	0.92 (0.03)	0.98 (0.01)	0.97 (0.02)
Cold	0.83 (0.12)	0.57 (0.19)	0.83 (0.08)	0.82 (0.07)	0.94 (0.03)	0.85 (0.13)

696

Biogeosciences Discuss., doi:10.5194/bg-2015-661, 2016
Manuscript under review for journal Biogeosciences
Published: 7 March 2016

Table C5. Median site-by-site RMSE of the energy fluxes per PFT and climate zones. ENF was evergreen needle leaf forest, DBF deciduous broadleaf forest, EBF Evergreen broadleaf forest, MF mixed forest, SHR shrubland, SAV Savannah, GRA Grassland, CRO cropland, WET Wetland, Trop Tropical, SubTrop Subtropical, Dry Dryland, Tmp Temperate, TmpCont Temperate-continental, Bor Boreal, Cold cold environment or Iceland covered by ice.

CAT	H ($MJm^{-2}d^{-1}$)		LE ($MJm^{-2}d^{-1}$)		Rn ($MJm^{-2}d^{-1}$)	
	RS	RS+METEO	RS	RS+METEO	RS	RS+METEO
ENF	1.09 (0.25)	1.16 (0.25)	1.00 (0.56)	1.02 (0.55)	1.27 (0.68)	1.26 (0.57)
DBF	1.30 (0.43)	1.31 (0.38)	1.22 (0.26)	1.14 (0.46)	1.11 (0.42)	1.24 (0.41)
EBF	1.14 (0.60)	1.29 (0.76)	1.55 (0.39)	1.60 (0.46)	1.33 (0.43)	1.14 (0.56)
MF	1.18 (0.44)	1.12 (0.42)	0.82 (0.37)	1.15 (0.54)	1.14 (0.45)	1.09 (0.43)
SHR	1.21 (0.46)	1.14 (0.28)	1.12 (0.41)	1.11 (0.56)	1.37 (0.80)	1.01 (0.43)
SAV	1.23 (0.25)	1.20 (0.22)	1.32 (0.56)	1.35 (0.30)	1.10 (0.33)	1.19 (0.60)
GRA	1.14 (0.35)	1.08 (0.47)	1.09 (0.34)	1.32 (0.54)	1.48 (0.83)	1.48 (0.90)
CRO	1.24 (0.45)	1.36 (0.33)	1.51 (0.61)	1.54 (0.35)	1.24 (0.52)	1.23 (0.26)
WET	0.97 (0.36)	1.22 (0.60)	0.88 (0.13)	0.90 (0.18)	1.42 (0.51)	1.65 (0.71)
Trop	0.98 (0.51)	1.19 (0.63)	1.60 (0.52)	1.62 (0.41)	1.33 (0.73)	1.03 (0.48)
SubTrop	1.28 (0.38)	1.32 (0.46)	1.36 (0.62)	1.36 (0.53)	1.40 (0.40)	1.33 (0.49)
Dry	1.07 (0.24)	1.05 (0.50)	1.21 (0.33)	1.27 (0.52)	1.61 (0.75)	2.02 (0.93)
Tmp	1.18 (0.23)	1.15 (0.33)	1.18 (0.43)	1.17 (0.49)	1.10 (0.36)	1.14 (0.47)
TmpCont	1.30 (0.42)	1.35 (0.37)	1.25 (0.41)	1.47 (0.37)	1.17 (0.65)	1.16 (0.54)
Bor	0.98 (0.23)	1.05 (0.26)	0.70 (0.26)	0.61 (0.20)	0.88 (0.31)	1.08 (0.50)
Cold	1.03 (0.36)	1.50 (0.55)	1.00 (0.23)	1.03 (0.45)	1.47 (0.18)	2.04 (0.19)

Biogeosciences Discuss., doi:10.5194/bg-2015-661, 2016
Manuscript under review for journal Biogeosciences
Published: 7 March 2016

701 **Table C6.** Median site-by-site absolute bias for energy fluxes. . ENF was evergreen needle leaf forest, DBF deciduous broadleaf forest,
702 EBF Evergreen broadleaf forest, MF mixed forest, SHR shrubland, SAV Savannah, GRA Grassland, CRO cropland, WET Wetland, Trop
703 Tropical, SubTrop Subtropical, Dry Dryland, Tmp Temperate, TmpCont Temperate-continental, Bor Boreal, Cold cold environment or
704 Iceland covered by ice.

CAT	H ($MJm^{-2}d^{-1}$)		LE ($MJm^{-2}d^{-1}$)		Rn ($MJm^{-2}d^{-1}$)	
	RS	RS+METEO	RS	RS+METEO	RS	RS+METEO
ENF	0.44 (0.40)	0.40 (0.33)	0.42 (0.41)	0.44 (0.49)	0.78 (0.63)	0.64 (0.61)
DBF	0.60 (0.35)	0.66 (0.35)	0.57 (0.56)	0.49 (0.50)	0.38 (0.28)	0.61 (0.49)
EBF	0.38 (0.48)	0.55 (0.46)	0.97 (0.79)	0.88 (0.70)	0.88 (0.51)	0.62 (0.43)
MF	0.48 (0.40)	0.26 (0.31)	0.34 (0.40)	0.64 (0.52)	0.56 (0.45)	0.56 (0.57)
SHR	0.34 (0.43)	0.47 (0.52)	0.41 (0.41)	0.50 (0.43)	0.62 (0.76)	0.44 (0.52)
SAV	0.68 (0.35)	0.56 (0.15)	0.63 (0.80)	0.40 (0.15)	0.27 (0.22)	0.63 (0.55)
GRA	0.51 (0.39)	0.40 (0.24)	0.38 (0.38)	0.57 (0.50)	0.97 (0.81)	0.81 (1.03)
CRO	0.23 (0.21)	0.24 (0.24)	0.36 (0.38)	0.41 (0.50)	0.66 (0.58)	0.68 (0.39)
WET	0.47 (0.51)	0.67 (0.37)	0.54 (0.41)	0.38 (0.21)	0.34 (0.34)	0.83 (0.78)
Trop	0.37 (0.51)	0.67 (0.47)	0.97 (0.79)	1.24 (0.82)	0.94 (1.10)	0.63 (0.60)
SubTrop	0.58 (0.59)	0.50 (0.39)	0.62 (0.58)	0.58 (0.56)	0.83 (0.71)	0.70 (0.55)
Dry	0.68 (0.62)	0.55 (0.56)	0.21 (0.14)	0.30 (0.26)	1.06 (0.55)	1.61 (0.91)
Tmp	0.38 (0.23)	0.34 (0.31)	0.49 (0.46)	0.56 (0.54)	0.65 (0.49)	0.68 (0.58)
TmpCont	0.49 (0.41)	0.40 (0.46)	0.44 (0.51)	0.53 (0.50)	0.69 (0.72)	0.61 (0.58)
Bor	0.33 (0.32)	0.38 (0.24)	0.22 (0.16)	0.23 (0.24)	0.38 (0.27)	0.50 (0.47)
Cold	0.43 (0.46)	0.71 (0.11)	0.56 (0.31)	0.39 (0.18)	0.30 (0.29)	0.86 (0.58)

Biogeosciences Discuss., doi:10.5194/bg-2015-661, 2016
Manuscript under review for journal Biogeosciences
Published: 7 March 2016

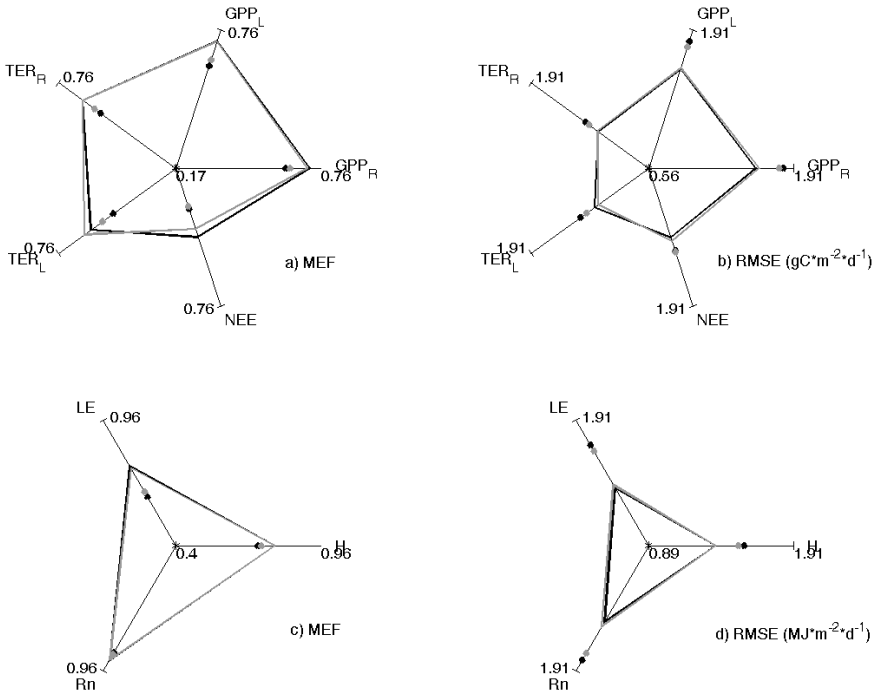

Fig. 1: Spider plot of MEF (first column) and RMSE (second column) for CO_2 (first row) and energy fluxes (second row) showing the consistency of prediction made by RS (Black line) and RS+METEO (grey lines) setups. The lines were the ensemble median estimate of ML; we also showed the performance of multiple regressions trained with RS (black point) and RS+METEO (gray points). GPP_R and GPP_L were respectively gross primary production estimated following Reichstein et al. (2005) and Lasslop et al. (2010), TER_R and TER_L the total ecosystem respiration estimated following Reichstein et al. (2005) and Lasslop et al. (2010), NEE net ecosystem exchange, H the sensible heat, LE the latent heat and Rn the net radiation.

Biogeosciences Discuss., doi:10.5194/bg-2015-661, 2016
Manuscript under review for journal Biogeosciences
Published: 7 March 2016

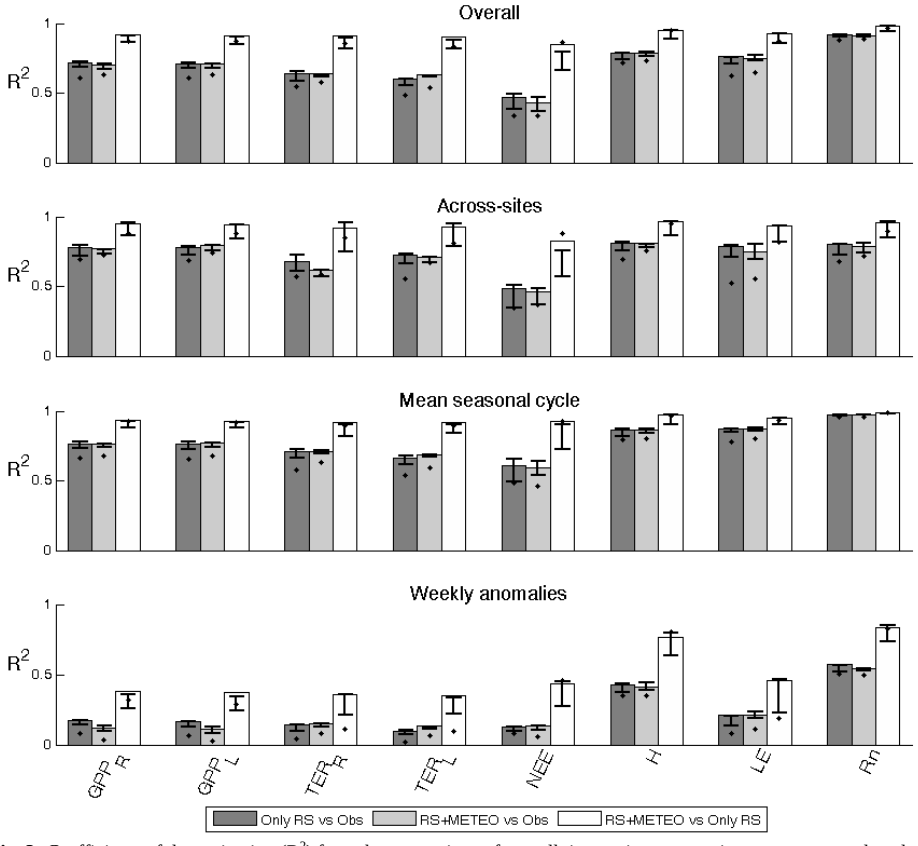

Fig. 2: Coefficients of determination (R^2) from the comparison of overall time series, across-sites, mean seasonal cycle, and the anomalies, in particular: the determination coefficients between predictions by the ensemble median estimate of RS setup and observation (dark grey bars), between predictions by the ensemble median estimate of RS+METEO setup and observation (light grey bars), and between the two ensembles median estimate (white bars). Whiskers were the higher and lower R^2 when the comparisons were made among the singular ML. The comparison of output by the multiple regressions was also shown (black points).

Biogeosciences Discuss., doi:10.5194/bg-2015-661, 2016
Manuscript under review for journal Biogeosciences
Published: 7 March 2016

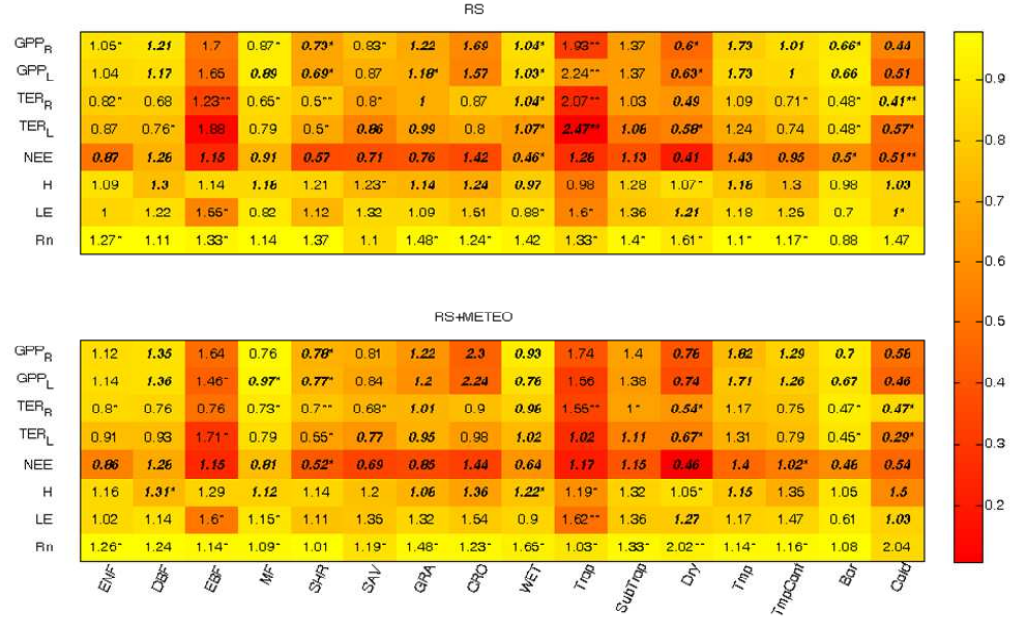

Fig. 3: Performance of FLUXCOM median estimates per climate zone and plant functional type (PFT). The colored matrices showed the median values of R^2 (red pixels for low R^2, yellow pixels for high R^2). Number indicated the RMSE (units of CO_2 fluxes were $gCm^{-2}d^{-1}$ and $MJm^{-2}d^{-1}$ in the case of energy fluxes). Oblique and bold font were used when the relative RMSE (normalized for the mean observed fluxes per PFT and climate zone) was greater than 0.5. The symbols '**' after RMSE were used when the weight of bias (estimated as the ratio between the square of median absolute bias and the MSE) was greater than 0.5, instead '*' symbols were used if the weight of bias was between 0.25 than 0.5. No symbols were used if the weight of bias is lesser than 0.25.

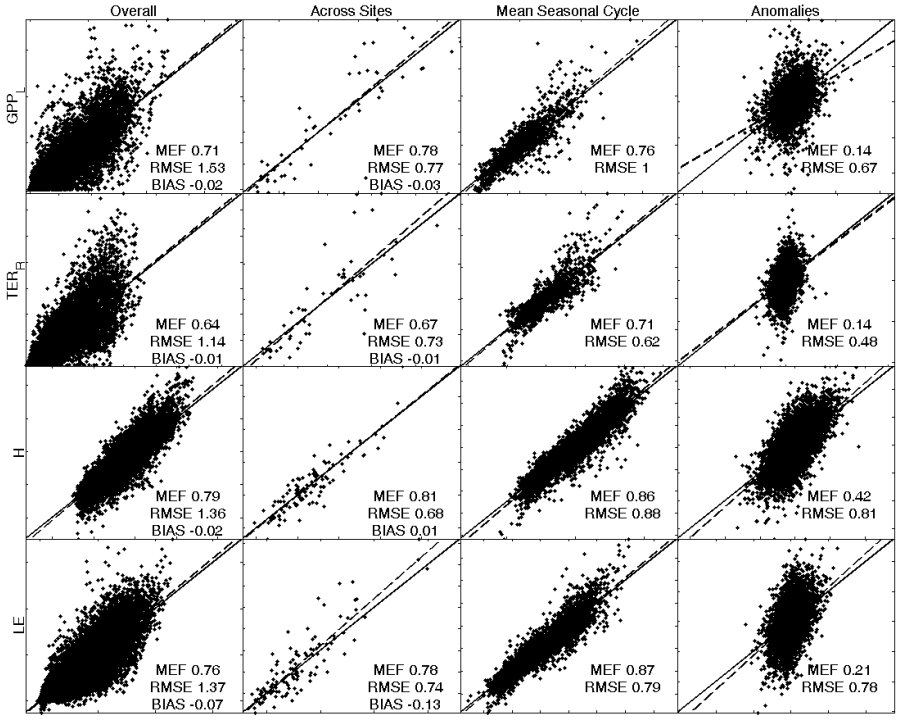

Biogeosciences Discuss., doi:10.5194/bg-2015-661, 2016
Manuscript under review for journal Biogeosciences
Published: 7 March 2016

Fig. B1. Scatterplots of observed data by eddy covariance (y-axis) and the median ensemble of modeled fluxes by RS setup (x-axis). The panels from left to right were the eight days predictions, the across sites variability, the mean seasonal cycle and the eight days anomalies. The fluxes considered here were GPP_L (first row), TER_R (second row), H (third row) and LE (fourth row).

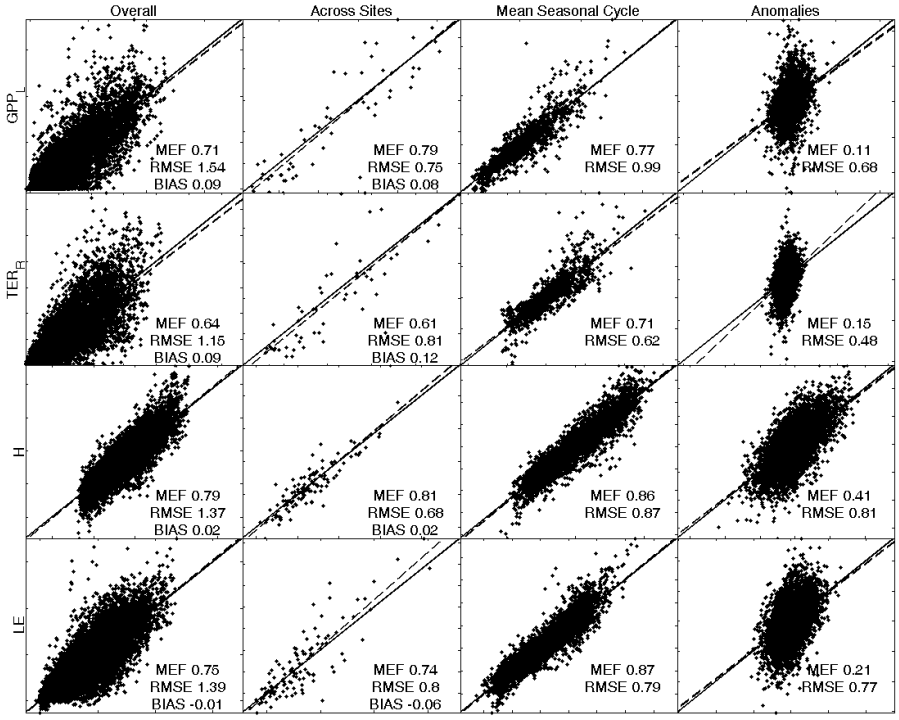

Fig. B2. As Fig. B1 but the predictions (x-axis) were obtained by the RS+METEO setup.